SLAC-PUB-1820
September 1976
(T/E)

CONNECTIONS BETWEEN LEPTON-INDUCED AND HADRON-INDUCED MULTIPARTICLE REACTIONS*

STANLEY J. BRODSKY

Stanford Linear Accelerator Center
Stanford University, Stanford, California 94305 USA

(Invited talk presented at the VII International Colloquium on Multiparticle Reactions, Tutzing/Munich, Germany, 21-25 June 1976.)

and

J. F. GUNION

Department of Physics
University of California, Davis, California 95616 USA

ABSTRACT

Jet production is studied as a link between hadron- and lepton-induced reactions and interpreted in terms of models of underlying quark dynamics. We discuss how fragmentation distributions, quantum number flow, the charged-momentum vector, and quark counting rules can discriminate among various possible jet structures. We also review recent work on the possible relationship of the rising hadron multiplicity to quark confinement and color gauge theories. A number of new tests of quark models in hadron, photon, and lepton collisions are discussed.

*Work supported in part by the Energy Research and Development Administration.

1. INTRODUCTION

One of the most striking indications of the underlying quark structure of hadronic matter has been the observation of jet production in e^+e^- annihilation.[1] The hadrons observed at SPEAR are produced with limited transverse momentum about a central axis which has the angular distribution (in both $\theta_{c.m.}$ and ϕ) expected for a pair of elementary Dirac particles. This phenomenon, together with the scaling behavior of the cross section, evidently reflects the virtual creation of the elementary spin one-half quark pairs which compose the electromagnetic current. Hadrons are then produced as the quark quantum numbers are neutralized; since the bound state wave functions have decreasing form factors, the hadrons are emitted at low transverse momentum relative to the jet axis.

Although we are fairly certain that "quark" jets are produced in e^+e^- annihilation, deep inelastic processes, and perhaps, as we discuss later, large p_T reactions, the paradoxical fact is that these jets are not so dissimilar from the jet-like systems produced along the beam directions in ordinary hadron collisions. Indeed, given the same available energy, the multiplicity and transverse momentum distribution of hadrons relative to the jet axis in lepton-induced reactions do not differ greatly from those of hadron-induced reactions. Further, the charged hadron multiplicity for electroproduction $\gamma(q^2) + p \rightarrow X$ is remarkably independent of q^2, as shown in Fig. 1, even as $q^2 \rightarrow 0$, thus bridging the gap between deep inelastic and ordinary meson-induced reactions. This is an example of the "correspondence principle" of Bjorken and Kogut[3] which postulates a smooth connection and essential similarity between

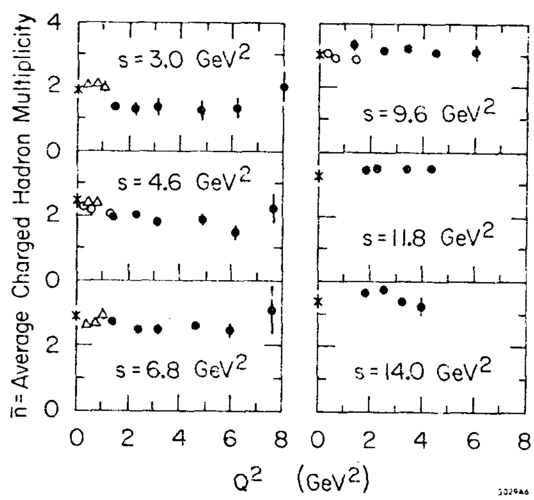

Fig. 1--The average charged-hadron multiplicity as a function of photon mass. (From Ref. 2.)

large and small q^2 reactions.

The paradoxical similarity between hadron- and lepton-induced multiparticle reactions leads one to wonder whether there is an underlying connection at the quark level. Certainly our usual descriptions of hadron dynamics (Regge and Pomeron expansions, multiperipheral and statistical models, etc.) are orthogonal to those of lepton-induced reactions (local currents, quark parton model, asymptotic freedom, etc.). Multiparticle production is generally believed to begin well before the interaction via a multiperipheral chain in hadron-induced reactions, whereas hadrons are supposed to be created in an inside-outside cascade in deep inelastic lepton processes. (See Section 7.) Still, if an underlying field theory such as quantum chromodynamics[4] (QCD) is correct, then there must be a common microscopic description of hadron production in both hadronic and leptonic processes. Jet structure is the apparent common link between these reactions and should be an important clue to the understanding of the underlying quark dynamics.

In this lecture we will explore the possible connections between hadron- and lepton-induced reactions, with special emphasis on jet and cluster production on the empirical side and models, such as the color gauge theory on the theoretical side. We also discuss the tools available for further identifying and distinguishing the various types of jets expected in these reactions.

2. FEATURES OF JET PRODUCTION

We can define a jet as a high momentum multiparticle system with limited transverse momentum $\vec{k}_\perp$ relative to the jet momentum $\vec{P}$ and scaling in the longitudinal Feynman (or light-cone variable)

$$x = (k_z + k_0)/(P_z + P_0) \to k_z/P_z \quad (\text{for } P_z \to \infty)\,. \tag{2.1}$$

Feynman scaling implies that the particle distribution

$$\frac{dN}{dx} = \frac{1}{\sigma_{inel}} \int \frac{d^3\sigma}{d^2k_\perp dx}\, d^2\vec{k}_\perp \tag{2.2}$$

is asymptotically independent of the total jet momentum. If $dN/dx \sim x^{-1}$ for $x \to 0$, i.e., dN/dy is flat in rapidity $y = \log x$, then the jet multiplicity grows logarithmically with jet momentum. The jets observed at SPEAR, where the jet axis is defined by minimizing the total $\vec{k}_\perp^2$, and x is taken as $k_\parallel / (\sqrt{s}/2)$, appear to satisfy these prerequisites.[1] As noted by Gilman,[5] the jets at PEP and PETRA could be very SPEAR-like, with a ratio of dimensions $\langle p_T \rangle / 15$ GeV ~ 0 (2%).

Jets have been identified in at least three other situations:

(i) There is good evidence that a similar type of quark jet is produced in the current fragmentation region in deep inelastic lepton scattering, $\ell p \to \ell' X$.[6] In particular, the shape of the fragmentation distributions dN/dx roughly agree in the fragmentation region with the SPEAR distributions, and the charge distributions of the current fragmentation region appear to reflect the underlying quantum numbers expected in the quark-parton model. This is discussed further in Section 3.

(ii) There is some evidence from the CERN-ISR[7] that a quark-like jet may be produced as the recoil system balancing the transverse momentum on the opposite side of a 90° high p_T meson trigger in $pp \to \pi^0 X$. There is evidence of limited transverse momentum (transverse to the production plane), rising away-side multiplicity, and a scaling distribution resembling the SPEAR and $ep \to eX$ distributions. See Fig. 2. (This must be regarded as only a tentative possibility since nonscaling behavior was recently reported for a 45° trigger by the CCHK[8]

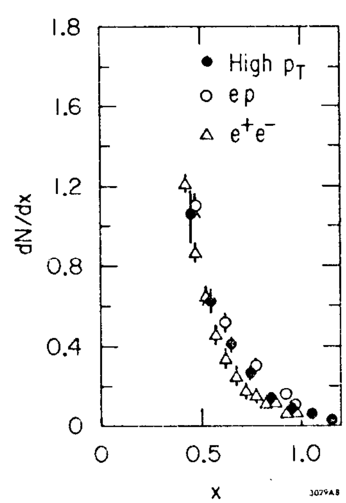

Fig. 2--Comparison of hadron fragmentation in $ep \to ehX$, $e^+e^- \to hX$, and pp collisions (on the side away from a π^0 90° trigger with $p_T \geq 2$ GeV). In the latter case $x = |p_h^T| / |p_{\pi^0}^T|$. (From Ref. 7.)

group.) It should be emphasized that the structure of the jet structure in high p_T reactions depends in detail on the underlying production mechanism.[9] A recoil quark jet is indeed expected for models based on elementary quark-quark scattering and also in the constituent interchange model (CIM)[10] which is based on elementary quark-hadron scattering, $qM \to qM$.

On the other hand, the system on the same side as the trigger high p_T particle cannot be directly identified with a quark jet. The trigger π is rarely accompanied by a second particle with substantial momentum. For example, for p_T (trigger) > 2 GeV the probability of a second pion on the same side with $p_T > 1.1$ GeV is less than 2%.[11] This is reflected in the constancy of the same-side multiplicity as the p_T of the trigger increases: $\langle n_{ch} \rangle$ (same side) = .85 ± .15 for $1 < p_T < 4$ GeV/c.[12] The associated multiplicity reported by the Pisa-Stony Brook collaboration[13] for $pp \to \pi^0 X$ at $\sqrt{s} = 53$ GeV, $\theta_{c.m.} = 90^0$ is shown in Fig. 3. Although the away-side jet multiplicity ($\phi \sim 180^0$) increases in the bin $|\eta| < .7$ opposite the trigger, little growth is seen on the same side ($\phi \sim 0^0$). Thus there is little evidence that the same-side system in high p_T reactions can be identified with a quark jet. The ISR results including the power law behavior and angular dependence seem to be consistent with a dominant $qM \to qM$ subprocess, where M is a meson cluster, as postulated in the CIM. However, as emphasized by Field,[11] the constancy of the same-side multiplicity does not preclude an underlying $qq \to qq$ subprocess because of the severe biasing of the large p_T trigger.

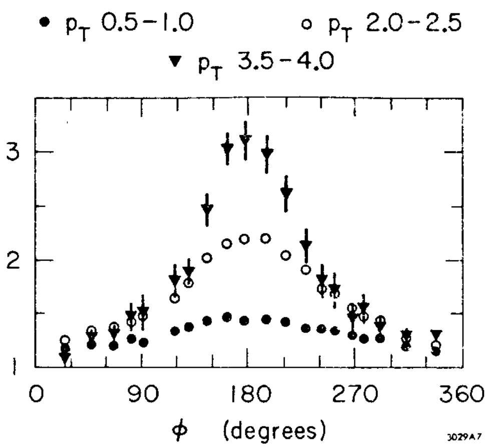

Fig. 3--Multiplicity distributions (normalized to low p_T events) for charged particles in the rapidity bin $|\eta|<0.7$ in association with a π^0 produced at 90^0 with $p_T > 0.5$ GeV. (From Ref. 13.)

An interesting question is how one can empirically distinguish the quark jet from a jet of hadronic parentage. For definiteness, we shall identify a "mesonic" jet or "cluster" as a system of $|q\bar{q}>$ color-singlet bound states. Since this system is already neutral in color there is no reason in a color model for the multiplicity of the system to increase with the jet momentum. Thus we expect x dN/dx to vanish at $x \to 0$, and the spectrum of masses in the meson cluster to have finite $<\mathcal{M}^2>$; i.e., $\rho(\mathcal{M}^2) = dN/d\mathcal{M}^2 \sim (\mathcal{M}^2)^{-1-\epsilon}$ with $\epsilon > 0$. On the other hand, if the cluster mass is unbounded, then there is no reason to think of the q and $\bar{q}$ of a meson system as being in any way bound to one another, just as in deep inelastic scattering, highly separated quarks are said to be free and independent of one another. In addition, quark-counting rules[14] do not directly apply to large angle scattering amplitudes involving meson systems of unbounded mass. In particular, a finite mass spectrum is also necessary to derive the scaling laws for high p_T reactions in the CIM, based on quark-hadron scattering, and the quark-fusion model of Landshoff and Polkinghorne,[15] based on model $q\bar{q} \to M\bar{M}$; otherwise there is no logical distinction between $q\bar{q} \to M\bar{M}$ and $q\bar{q} \to q\bar{q}$ with a subsequent quark-loop neutralization. Using this criterion, the continuing rise of the multiplicity on the away side of a high p_T trigger in $pp \to \pi X$ would favor the identification of the away side system as a quark jet rather than a mesonic jet or cluster.[16]

As an aside we note that it is natural to assume that the fragments of a quark jet are the limited-mass mesonic or baryonic clusters (color singlet $|\bar{q}q>$ and $|qqq>$ bound states and resonances) which subsequently decay to the observed hadrons. However, because of phase space suppression, the leading pions produced at x near one are produced directly rather than via the decay of a cluster or resonance. Whether a universal cluster structure can be identified in all jet phenomena is an interesting empirical question.

(iii) Historically, the prototype for scaling-jet structures is normal inclusive production, $H_1 + H_2 \to H_3 + X$. The final state hadrons are distributed along the initial center-of-mass axis with limited p_T, with $<p_T^2>$ ~ constant or growing slowly with s. The distribution dN/dx ($x = k_z^{c.m.}/k_z^{max}$) was thought to exhibit scaling until recent very high energy ISR experiments which suggest a "plateau" rising slowly with s.[17] If there is a common origin for jet structure, such rising plateaus should also be seen in deep inelastic and large p_T reactions at high enough jet momentum.

The striking similarity between the lepton- and hadron-induced jets is most apparent in the universal nature of the multiplicities. A phenomenological fit was performed by Albini et al.[18] to the proton-proton multiplicity over the entire available energy range. The best χ^2 fit is (see Fig. 4)

$$\langle n_{ch} \rangle_{pp \to X} = 2.50 + 0.28 \, \ell n \sqrt{s_a} + 0.55 \, \ell n^2 \sqrt{s_a} \qquad (2.3)$$

where $\sqrt{s_a}$ is the available energy $\sqrt{s_a} = \sqrt{s} - M_1 - M_2$ for additional particle production. Figures 5 and 6 show that the same parametrization also fits meson-proton collisions, and inclusive processes such as $\pi^- p \to pX$. However, the remarkable fact is that the same function

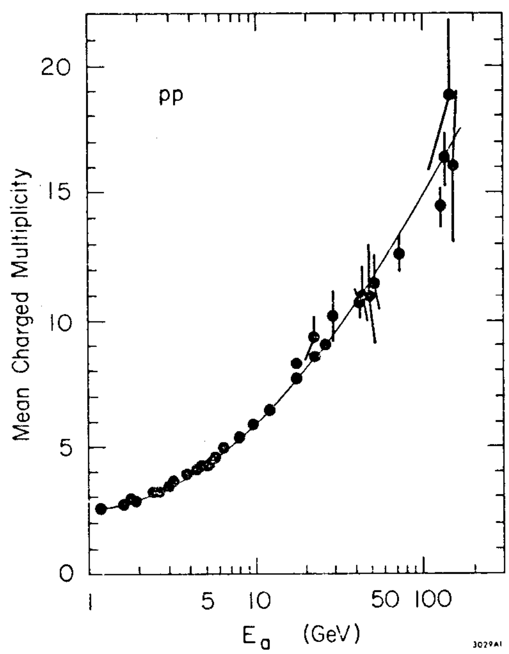

Fig. 4--The mean charged multiplicity in pp collisions versus available energy $E_a = \sqrt{s} - 2M_p$. The curve is the best fit, Eq. (2.3). (From Ref. 18.)

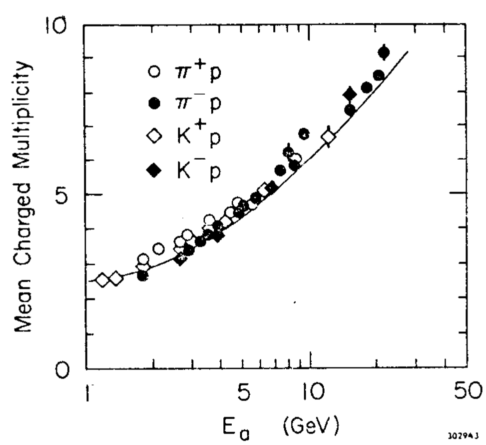

Fig. 5--Mean charged multiplicity in meson-proton collisions versus $E_a = \sqrt{s} - M_p - M_M$. The curve is the fit to the pp multiplicity. (From Ref. 18.)

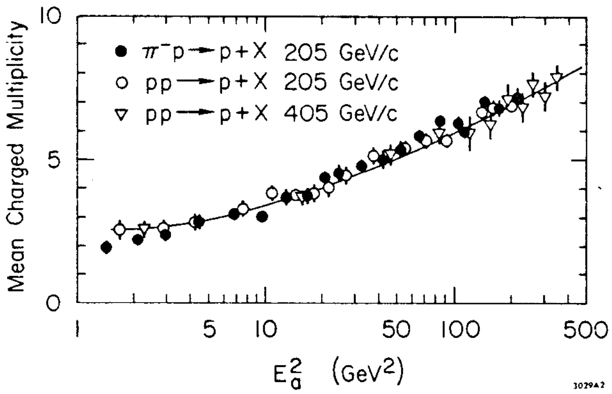

Fig. 6--Associated mean charged multiplicity in diffractive inclusive reactions versus $\sqrt{s_a} = M_X - M$. (From Ref. 18.)

$\langle n_{ch}\rangle_{pp\to X}$ also fits the observed multiplicity in $e^+e^- \to X(s_a = s)$ and in $\ell p \to \ell' X$ ($s_a = W^2 - M_p^2$), although we should note that the energy range in these cases is more restricted (see Figs. 7 and 8). Figures 1 and 8 show the q^2 independence of $\langle n_{ch}\rangle_{ep\to eX}$ at fixed $s = W^2$ and the comparison with $\langle n_{ch}\rangle_{\gamma p\to X}$.

An important distinction between the lepton- and hadron-induced jets is the different power law behavior for hadron fragmentation at $x \to 1$. We will discuss this and other tools for distinguishing the underlying quark jet structure in Sections 3 and 10. Of course one must also not ignore the fact that in e^+e^- annihilation thresholds for new physics (charm, heavy leptons) are crossed as s increases, whereas in $\ell p \to \ell' X$ such thresholds, if present, are not of such importance. We shall attempt later to explain why jet

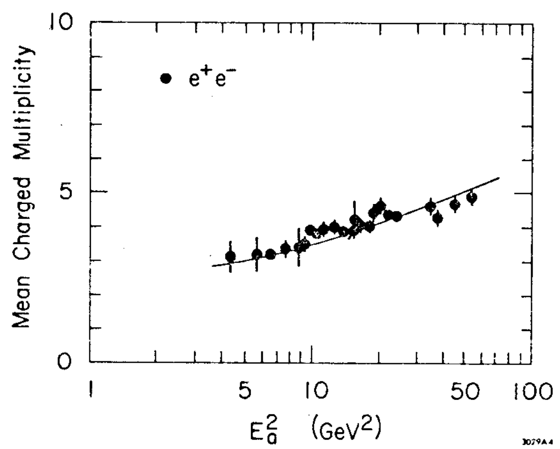

Fig. 7--Mean charged multiplicity in e^+e^- annihilation versus $s_a = s$. The curve is the best fit to pp → X. (From Ref. 18.)

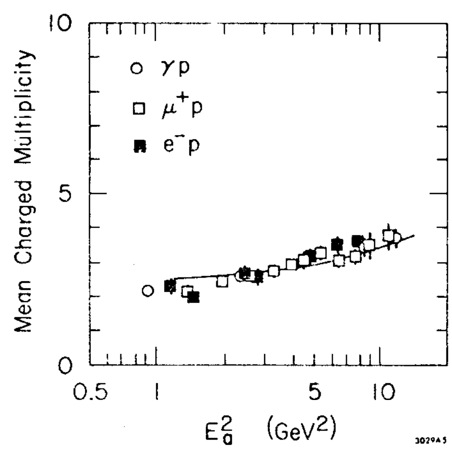

Fig. 8--Mean charged multiplicity in deep inelastic scattering. and photoproduction. The curve is the best fit to pp → X. (From Ref. 18.)

multiplicity universality is maintained,[19] i.e., behaves smoothly upon crossing a new quark flavor threshold, despite this difference.

3. QUANTUM NUMBER RETENTION IN LEPTON-INDUCED REACTIONS

One of the most interesting questions concerning quark jets is whether, as first suggested by Feynman,[20] the quark quantum numbers are retained in the quark fragmentation region ($x \neq 0$) (averaging over events). This is only an ansatz, since theoretical models have been constructed in which this is not true for the retention of charge and strangeness, although it is still true for I_z.[21] In any case, this is an interesting question to examine empirically.

The simplest test of the charge retention ansatz is the charged-current reaction $\nu p \to \mu^- h^{\pm} X$, which is most easily visualized in the W^+p c.m. system. Figure 9 corresponds to the usual "handbag" diagram of the quark-parton model. (The initial c.m. momentum is $p^{\text{init}}_{\text{c.m.}} = (s+Q^2)/2\sqrt{s}$ where $s = (p+q)^2$, $q^2 = -Q^2$.) The condition $p^{\text{final}}_{\text{c.m.}} = \sqrt{s}/2 = (1-x)p^{\text{init}}_{\text{c.m.}}$ for the spectator fragments of the target, gives $x = x_{Bj} = Q^2/(s-Q^2) = -q^2/2p\cdot q$. For $x_{Bj} \gtrsim 0.2$, essentially only the d quark interacts, producing, as in Fig. 10a, two jets, a u quark in the current (W^+) fragmentation region, and a jet with the quantum numbers of two u quarks, in the proton

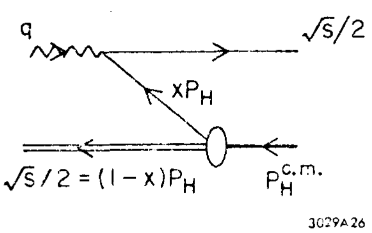

Fig. 9--Parton model for deep inelastic lepton scattering in the γp or Wp c.m. system.

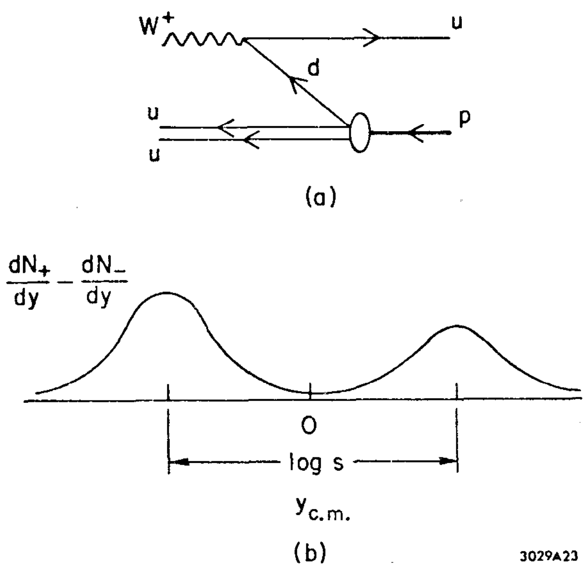

Fig. 10--(a) The initial quark distribution for $\nu p \to \mu^- X$ in the W^+p c.m. (b) Expected distribution in rapidity of the hadronic charge density for $\nu p \to \mu^- X$ in the W^+p c.m.

fragmentation region. For $x_{Bj} \lesssim .2$, the $\bar{u}$ and s quarks in the sea also interact with the W^+ producing final states with a charge breakup of (1/3, 5/3), and (2/3, 4/3) in the two hemispheres, respectively. Thus, the most naive expectation is that at least twice as much charge should be found in the proton-fragmentation region, which for $s \to \infty$ should separate in rapidity from a logarithmically growing neutral central plateau and the W-fragmentation region (see Fig. 10b). Even at low energies, we expect a 2:1 ratio of charge in the two hemispheres.

The results of the University of Michigan hydrogen bubble chamber experiment[22] at FNAL at $s \gtrsim 25$ GeV^2 are shown in Fig. 11. The distribution of the sum of charged particles $h^{\pm}$ in both y and p_T is similar to that seen in ordinary $pp \to hX$ reactions. However, the difference $dn^+/dy - dn^-/dy$ clearly shows a charge asymmetry effect of the type expected. This skewing is remarkable, if one considers that in ordinary hadron reactions (e.g., $\pi^+ p \to X$) the average charge of the beam and target fragments is close to the charge of the beam and target particles (at least at low p_T).

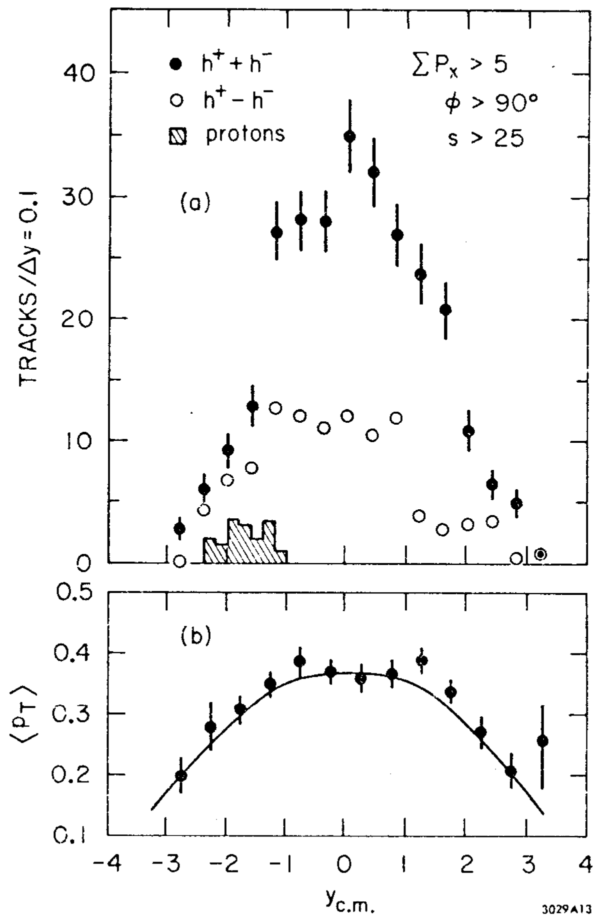

Fig. 11--(a) Distributions $(dN_+ \pm dN_-)/dy$ of charged particles observed in $\nu p \to \mu^- X$ in the W^+p c.m. (b) The average transverse momentum of charged hadrons observed in $\nu p \to \mu^- X$. The curve is taken from pp reactions. (From Ref. 22.)

A comparison of the Feynman-Bjorken model[23] (which includes an additional contribution from "hole" fragmentation) with the neutrino data has been given by Vander Velde and

Seidl.[22] In the color model[19] discussed in Section 7 there is no distinctive "hole" contribution, since the hadron production only begins after the color is separated; the simplest predictions as discussed above for the quantum number distribution should be applicable.

Another test of charge retention is the π^+/π^- ratio in $ep \to e\pi^\pm X$. The expected ratio in the current fragmentation region in the quark parton model is[24]

$$\frac{N_{\pi^+}(x,z)}{N_{\pi^-}(x,z)} = \frac{\sum_q e_q^2 G_{q/p}(x)\, D_{\pi^+/q}(z)}{\sum_q e_q^2 G_{q/p}(x)\, D_{\pi^-/q}(z)} \tag{3.1}$$

where $G_{q/p}$ and $D_{\pi/q}$ are the usual proton and quark fragmentation functions, $x = -q^2/2p\cdot q$ and $z = p_\pi^{c.m.}/p_\pi^{max} \cong 2p_\pi^{c.m.}/\sqrt{(p+q)^2}$. A typical test involves fixing x and integrating over a range of z. Assuming the $q\bar{q}$ sea is SU(3)-symmetric and described by s(x), one obtains from charge symmetry[24]

$$R_\pi = \frac{N_{\pi^+}(x)}{N_{\pi^-}(x)} = \frac{4\eta u(x) + d(x) + (5\eta+7)s(x)}{4u(x) + \eta d(x) + (5\eta+7)s(x)}, \tag{3.2}$$

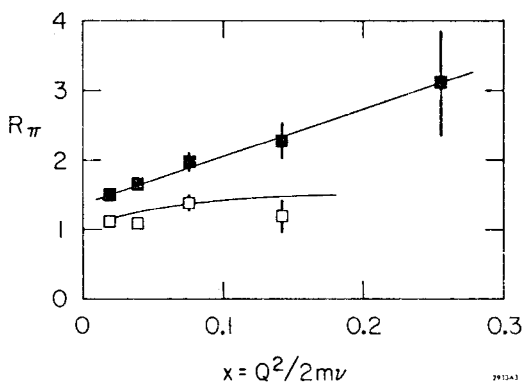

Fig. 12--Ratio of π^+ to π^- in the virtual photon fragmentation direction as a function of the Bjorken variable. The electroproduction data is for the range $0 < p_T^2 < 0.64$ GeV^2, $15 < s < 31$ GeV^2, and $0.4 < z < 0.85$. (From Ref. 26.)

where

$$\eta = \int_a^b dz\, D_{\pi^+/u}(z) \Big/ \int_a^b dz\, D_{\pi^+/d}(z) \tag{3.3}$$

is the "favored to unfavored" ratio. Using the distribution function of Ref. 25, J. Martin[26] finds good fits to the data (see Fig. 12) if $\eta = 5.9 \pm 0.5$ for $0.4 < z < .85$.

A critical test of the quark model based on charge retention has been proposed by Bjorken and Miettinen.[27] Assuming again that the current fragmentation region in $\nu p \to \mu^- X$ is dominated by the u quark (Fig. 10a) one can obtain the ratio $\eta(z) = D_{\pi^+/u}(z)/D_{\pi^-/u}(z)$ from the existing data. A simple fit[27] gives $\eta(z) = [6(1-z)]^{-1}$. (We note that $(1-z)^{-1}$ is the kinematic dependence expected from ρ^0 decay to π^- assuming $D_{\rho^0/u}(z)$ and $D_{\pi^+/u}(z)$ have the same z dependence.) Using this fit for $\eta(z)$ they estimate that the two meson charge correlation in e^+e^- annihilation should have the ratio

$$\frac{e^+e^- \rightarrow \pi_1^+\pi_2^+X}{e^+e^- \rightarrow \pi_1^+\pi_2^-X} \sim 0.12 \quad \text{for } x_1+x_2 > 0.5$$

where π_1 and π_2 are in opposite jets. Such a small ratio arises from Eq. (3.1) and the fact that on an event by event basis the jets arise from a $q\bar{q}$ pair of a given type.

It is clearly also of interest to examine the retention of other charges such as baryon number in the deep inelastic reactions. A further test of the Feynman ansatz in $e^+e^- \rightarrow \gamma h^\pm X$ is discussed in Section 4. We also discuss the construction of a charged-current vector for jets in Section 6.

4. HARD PHOTON TESTS OF QUARK JET STRUCTURE

It is usually argued that only highly virtual photons can probe the short distance structure of the current within hadrons. In fact, when large momentum transfer is involved, even real photons are sensitive to the underlying hadronic structure. Examples of this are (a) deep inelastic Compton scattering, as discussed by Bjorken and Paschos,[28] (b) the asymmetry[25] $\sigma(e^+p \rightarrow \gamma e^+X) - \sigma(e^-p \rightarrow \gamma e^-X)$, which measures the sum of charges cubed of the quarks, (c) the fixed pole at j = 0 in the elastic Compton scattering amplitude,[30] which is predicted to be the dominant contribution at large t, and (d) fixed angle scaling laws involving real photons. In particular, dimensional counting rules predict $s^7 d\sigma/dt(\gamma p \rightarrow \pi p) \rightarrow f(\theta_{c.m.})$ at large s. A recent test of this is shown in Fig. 13. If vector dominance were to hold here, the expected power would be s^{-8} at fixed $\theta_{c.m.}$.

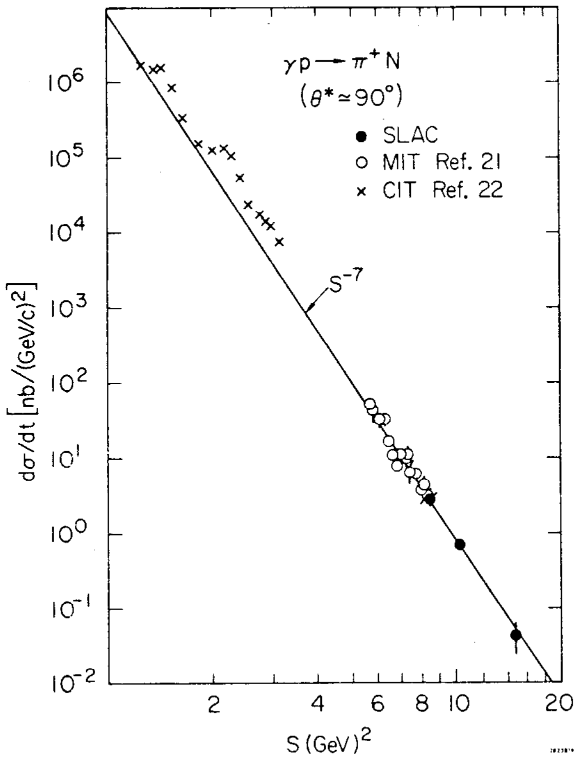

Fig. 13--$d\sigma/dt$ ($\gamma p \to \pi^+ n$) at $\theta = 90^0$ versus s. The line shows the s^{-7} quark counting prediction. (From Ref. 32.)

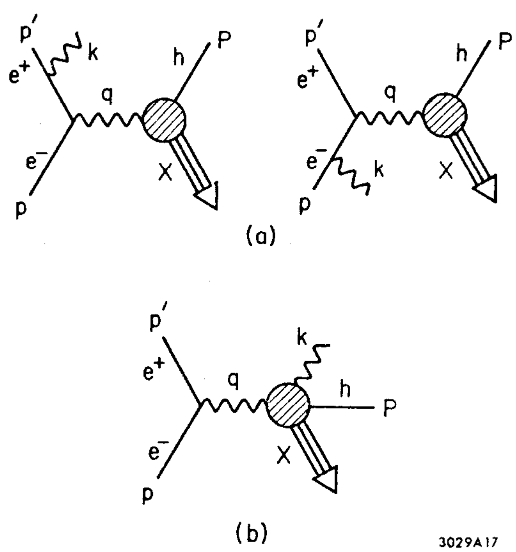

Fig. 14--Feynman diagrams for $e^+e^- \to \gamma h^{\pm} X$. The interference of (a) and (b) gives a charge asymmetry. (From Ref. 36.)

A particularly clear example of the difference between real-photon and meson production is the inclusive production ratio for γ to π at large p_T. Dimensional counting and the CIM predicts the ratio of inclusive cross sections for any beam and target:[33,34]

$$R(\gamma/\pi) \sim \alpha p_T^2 f(x_T, \theta_{c.m.}) \qquad (4.1)$$

since one less active field can be involved. This type of behavior was observed by a Santa Barbara group at SLAC[35] for $\gamma + p \to \gamma, \pi + X$. Further discussion is given by Farrar and Frautschi.[34]

An intriguing quark-parton model test involving real photon is the measurement of the charge asymmetry[36]

$$d\sigma(e^+e^- \to h^+\gamma X) - d\sigma(e^+e^- \to h^-\gamma X)$$

where the photon is detected at large p_T relative to the hadron $h^{\pm}$ direction. To lowest order in α the cross section arises from the interference of the amplitudes for the diagram of Fig. 14a with the "Compton" amplitude of Fig. 14b. The interference is proportional to

$$\langle 0 | J_\mu | h, X \rangle \langle h, X | T^*(J_\mu, J_\nu) | 0 \rangle \ .$$

For $k \cdot p_H$ large, contributions such as Fig. 15c are negligible in the scaling limit, leaving only the quark-current contributions shown in Figs. 15a and 15b. In the scaling region one easily finds that the ratio of hadron asymmetry (for the same kinematics) is simply[36]

$$R_h^{(3)} = \sum_q \frac{e_q^3}{e_\mu^3} \left[D_{h^+/q}(x) - D_{h^+/\bar{q}}(x) \right] \quad (4.2)$$

where the sum is over all contributing quark fields and $x = 2q \cdot p_h / q^2$ where $q^\mu = (p_{e^+} + p_{e^-} - k)^\mu$.

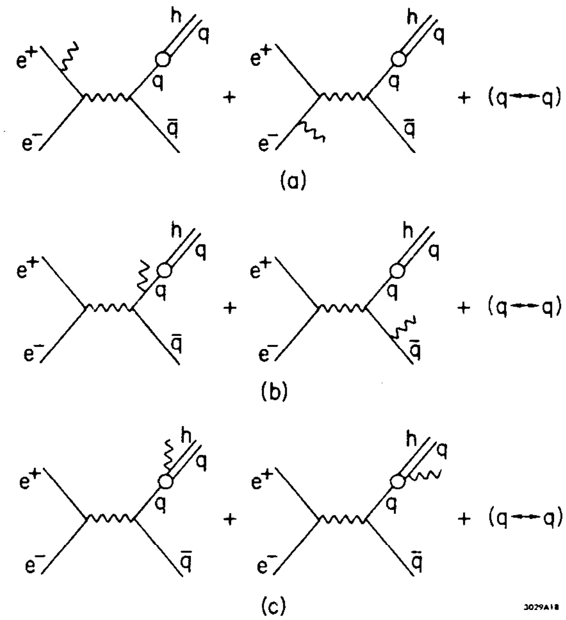

Fig. 15--Quark model diagrams for $e^+e^- \to \gamma h^\pm X$.

If the photon is not detected, the hadron asymmetry in $e^+e^- \to hX$ (from two-photon annihilation and radiative corrections is small (of order $8(\alpha/\pi) \log (\tan \frac{\theta}{2})$). Also, at SPEAR energies ($\sqrt{s} < 8$ GeV) weak-electromagnetic interference effects yield a small asymmetry (< 1%). Once the hard photon is detected, however, the electromagnetic asymmetry becomes maximal [$\sim 0(\cos\theta)$]. The background from π^0 and η^0 decay should be suppressed when the photon is detected at large p_T relative to the hadron jet because of Eq. (4.1).

There are numerous kinds of tests of scaling laws, quark-quantum numbers, fragmentation functions, color thresholds, etc., made possible by Eq. (4.2) which are discussed in detail in Ref. 36.

If we adopt Feynman's ansatz[20] that the quantum numbers of the quark are retained in its fragmentation region ($x \neq 0$) then for any conserved quantity λ,[36]

$$\sum_h \lambda_h (n_{h/q} - n_{\bar{h}/q}) = \sum_h \lambda_h \int_0^1 dx\, [D_{h/q}(x) - D_{\bar{h}/q}(x)] = \sum_{h,\bar{h}} \lambda_h n_{h,q} = \lambda_q \quad (4.3)$$

i.e.,

$$\sum_h \lambda_h \int_0^1 dx\, R_h^{(3)}(x) = \sum_q \lambda_q\, e_q^3/e^3 \tag{4.4}$$

e.g., for λ = the electromagnetic charge, we obtain a sum rule for $\sum_q (e_q/e)^4$. For a proton target this should be 34/27 above the charm threshold and 6 above the Han-Nambu color threshold.[37] The sum over h includes leptons if weak decays are included. An analogous sum rule also holds for the decay of a heavy lepton.

5. CHARGE RATIO IN INCLUSIVE PHOTOPRODUCTION

If real photons behave as vector mesons, then one would expect $\gamma p \to \pi^{\pm} X$ to be independent of the meson charge in the photon fragmentation region. The recent experiment of Boyarski et al.[38] at SLAC (see Fig. 16) for x_F = .77, s = 36 GeV^2 shows that this is false when the pion is detected at large p_T (> 0.8 GeV)

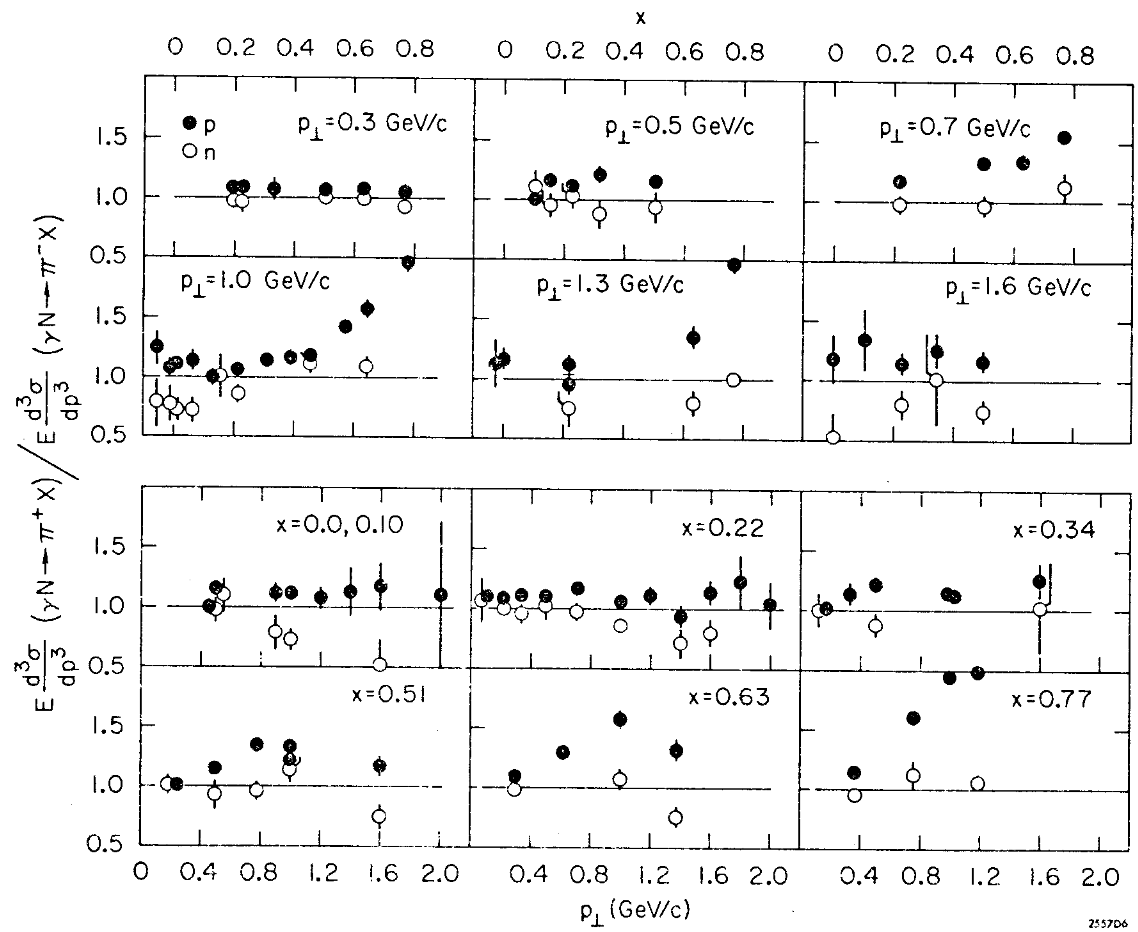

Fig. 16--Ratio of π^+ to π^- inclusive photoproduction in the photon fragmentation region. (From Ref. 38.)

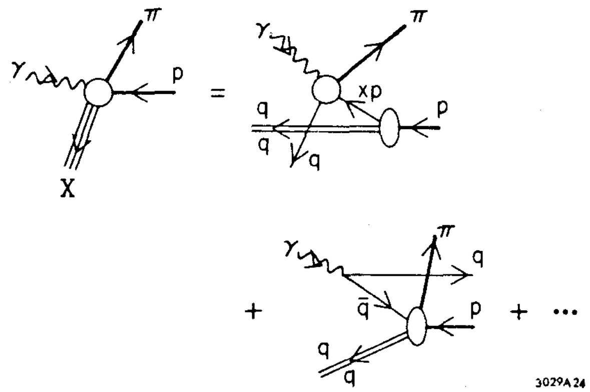

Fig. 17--Quark model diagrams for large p_T pion photoproduction. Diagram (a) is based on a $\gamma q \rightarrow \pi q$ large angle subprocess. Diagram (b) involves a $\bar{q}p \rightarrow \pi(qq)$ large angle subprocess.

relative to the photon direction; the proton charge has an important effect. One simple model which displays the influence of the valence quark charges is shown in Fig. 17a. The large p_T pion is assumed to be created by a $\gamma q \rightarrow \pi q$ subprocess. Allowing for virtual photons, the usual Bjorken infinite moment fraction x_{Bj} is defined by the mass-shell condition

$$\overset{\text{"s"}}{(xp+q)^2} + \overset{\text{"t"}}{(q-p_\pi)^2} + \overset{\text{"u"}}{(xp-p_\pi)^2} = q^2 \; ; \qquad (5.1)$$

i.e.,

$$x = x_{Bj} = \frac{-q^2 + 2q\cdot p_\pi}{2q\cdot p - 2p\cdot p_\pi} = \frac{-t}{\mathcal{M}^2 - t} \qquad (5.2)$$

which is a universal form for the Bjorken variable. Typically, $x_{Bj} = 0.2$ at $p_T = 1$ GeV for the Boyarski et al. data. Thus the growth of the π^+/π^- ratio is readily understood from the dominance of valence quark effects and the behavior of the u/d quark ratio as p_T and x_{Bj} increase. As usual, one expects $\pi^+/\pi^- \rightarrow 1$ at $p_T \rightarrow 0$ ($x_{Bj} \rightarrow 0$) where the sea quarks dominate.

We can conclude from this discussion that large p_T can produce long range charge correlations in rapidity, and that even real photons probe the proton charge in the large p_T region. Much more work in photoproduction and electroproduction is needed, including the simultaneous analysis in both the photon mass and transverse momentum variables.[39] An important check of the parton model based on Fig. 17a is to confirm whether the target charge effect is controlled solely by x, as defined in Eq. (5.2), and whether the inclusive cross section is proportional to νW_2^p.

It should be noted that there can be important contributions to photo- and electroproduction cross sections from non-leading diagrams at the exclusive edge of phase space, $\epsilon = \mathcal{M}^2/s \to 0$. For example, at SLAC energies $E_\gamma < 20$ GeV, diagrams of the type indicated in Fig. 17b can be expected to dominate at large p_T since the full proton momentum contributes to the large angle production process. These diagrams also favor π^+ over π^- production. Indeed, as discussed in Refs. 35 and 40, the power law behavior in ϵ and p_T observed in the SLAC experiments, in comparison with predictions based on the dimensional counting rules,[40] indicates that Fig. 17b rather than Fig. 17a gives the dominant contribution.

6. THE CHARGE-MOMENTUM VECTOR[41]

It is interesting to consider other quantities which can most simply characterize the nature of a multiparticle jet. For example, we can define the "charge-momentum vector"[41]

$$J^\mu = \sum_h e_h p_h^\mu \tag{6.1}$$

where the sum extends over all the charged hadrons in the jet. Because of the charge cancellations, J^μ is primarily a measure of the leading, rather than wee, hadrons in the jet, thus providing a convenient parametrization of the quark jet direction. This can be useful for tests of the angular distributions, and charge asymmetries from weak and electromagnetic effects. For example, for e^+e^- annihilation, the deviation of $\langle J^\mu \rangle$ from zero (averaged over all events at a given s) can be a sensitive test of the order (α^3) and weak-electromagnetic interference contributions. The spin 1/2 angular distribution $1 + \cos^2\theta$ implies

$$\langle J_z^2 \rangle : \langle J_x^2 \rangle : \langle J_y^2 \rangle = 4:3:3 . \tag{6.2}$$

The values and energy dependence of $\langle J_0^2 \rangle$ and $\langle \vec{J}^2 \rangle$ in e^+e^- annihilation may provide clues to the nature of quark jets and the hadron formation process. At the quark level $\vec{J}_q = 2e_q\vec{p}_q$, and $J_q^o = 0$. Averaging over quarks, this gives the scaling behavior,

$$\langle J_\mu^2\rangle_q \to \frac{s \sum_q e_q^4}{\sum_q e_q^2}, \quad \langle J_0^2\rangle_q = 0 . \tag{6.3}$$

Correspondingly, at the hadron level, we expect $\langle J_\mu^2\rangle/s \sim$ const, and $\langle J_0^2\rangle/\langle J_\mu^2\rangle$ to be a small, interesting ratio. Predictions for the value of $\langle J_\mu^2\rangle/s$ are quite model-dependent, but we can speculate that $\langle J_\mu^2\rangle = \lambda\langle J_\mu^2\rangle_q$ where λ is a (flavor- and s-independent) measure of how effectively the quark current is conveyed to the hadron current. [The constant λ is also related to the ratio of charged to total hadron energy.] If this is the case, we expect $\langle J_\mu^2\rangle/s$ to change by a factor of 17/15 when the charm threshold is passed. The effects of a heavy lepton can also be readily analyzed in terms of the charged-momentum vector. An alternative quantity to Eq. (6.1) with similar properties is the "convection" current $J^\mu_{conv} = e_h V_h^\mu$ where $V_h^\mu = p_h^\mu/m_h$.[42]

It is clear that vector quantities such as J^μ (and generalizations based upon other conserved quantum numbers) can provide very useful parametrizations of the jet momentum and its quantum numbers. It should be a useful tool for analyzing the jets in lepton and hadron-induced reactions, and a convenient parameter to compute in theoretical models.

7. HADRON MULTIPLICITY AND QUARK CONFINEMENT[19]

We will now turn to a study of the relationship between hadron production in various processes and its possible connections to an underlying quark theory. An interesting hypothesis is that the rising hadron multiplicity is due to the necessity of confining quark quantum numbers. (In contrast, the production of decaying quarks or heavy leptons would result in a finite, fixed multiplicity.) We will consider a specific realization of this hypothesis using the language of color SU(3)[quantum chromodynamics (QCD)] and color confinement, although the basic features are more general.

The idea that hadron production in e^+e^- annihilation is a response to the initially rapid separation of quark and antiquark quantum numbers and the polarization of the vacuum is an old one.[43] The approach given here can be considered the QCD generalization of the bremsstrahlung model of Stodolsky.[44] Clearly, whenever color "charges" are forced to separate, they radiate soft, colored gluons. The multiplicity of radiated gluons is then a function of the color quantum numbers of the separating objects and rises with increasing relative rapidity, as is the case in the analogous quantum electrodynamics calculations. The essential difference in QCD is that we presume that the intermediate gluons eventually materialize into hadrons in such a way that the hadron multiplicity is a direct, monotonic, possibly linear function of the gluon multiplicity. Thus the separation of color, combined with the necessity of confining color, naturally leads to a rising hadron multiplicity. Further, two processes with the same initial color-current configuration will produce the same multiplicity in the final hadronic state.

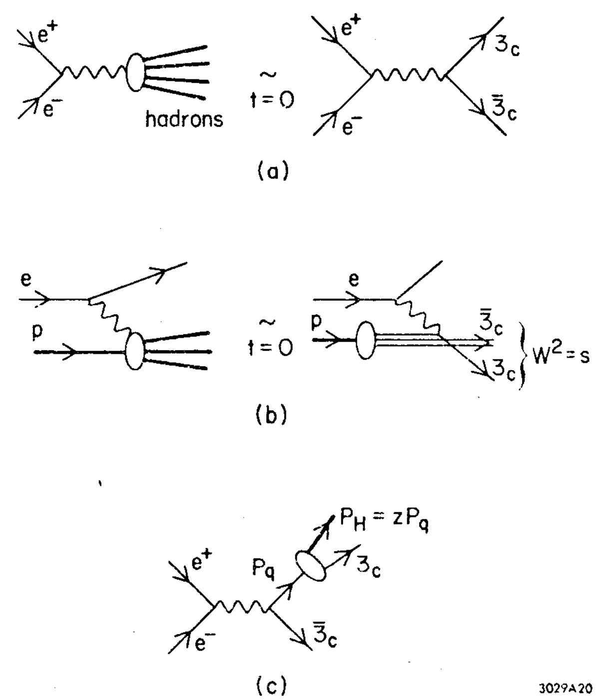

Fig. 18--Hadron production in (a) $e^+e^- \to X$, (b) $ep \to e'X$, (c) $e^+e^- \to H + X$. Each event begins with the timelike separation of a 3 and $\bar{3}$ of SU(3) color.

Let us first consider the general implications of this picture for hadronic multiplicity in e^+e^- annihilation and then relate it to deep inelastic and hadron scattering. The various stages of the process for e^+e^- annihilation arise as follows. Initially, a 3 and $\bar{3}$ of SU(3) color are produced and begin to separate (see Fig. 18a), giving rise to a gluon multiplicity $\langle n_g \rangle = f(3,\bar{3},s)$

which increases with log s. Assuming the number of hadrons is a monotonic function of the number of gluons, we can write

$$\langle n_{had} \rangle_{e^+e^- \to X} = n_{3\bar{3}}(s) \tag{7.1}$$

Other multiplicity moments will also depend on the initial separation of the color current. It is important to note that the rising contribution to the hadron multiplicity is flavor-independent. Valence effects due to quark flavor and mass can affect the leading particles in the fragmentation region, but beyond threshold they are energy-independent and of order one. Interestingly, despite the effects of possible heavy lepton production and charm meson decay, $\langle n \rangle_{e^+e^- \to X}$ above the charm threshold at $\sqrt{s} = 4$ GeV does seem to be a smooth continuation (Fig. 19) of the rising multiplicity below threshold, except, perhaps, for a temporary slowdown just above threshold where the relative rapidity of the colored charm quark is low. Notice also that if ψ decay proceeds via the initial production of an up or down quark pair, then $\langle n \rangle_{e^+e^- \to X}$ should be continuous at that point. The data are consistent with such continuity.[45]

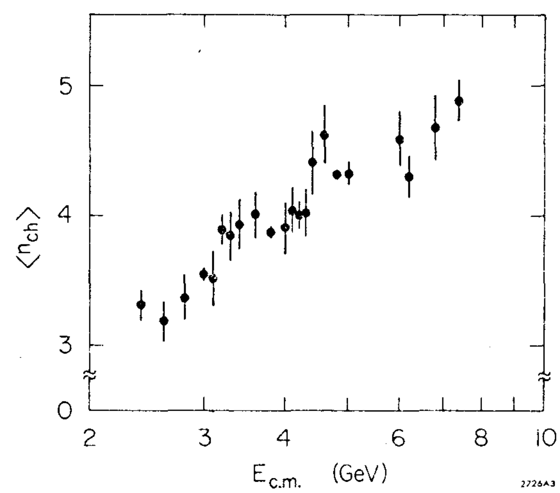

Fig. 19--Average charged multiplicity in $e^+e^- \to X$. (From Ref. 45.)

The color model for multiplicity can be readily applied to deep inelastic lepton-hadron scattering. The quark-parton model representation of the inelastic cross section on a nucleon target is indicated in Fig. 18b. For $x = -q^2/2p\cdot q \gtrsim 0.2$, we can take a simple three-quark Fock space representation of the nucleon. Again, each event begins with the initial separation of color: after the current interacts with the color-singlet hadron, a quark color-triplet is sent along $xp+q$, leaving behind a $\bar{3}$ of color with momentum $(1-x)p$, giving an invariant separation of color with $s = W^2 = (p+q)^2$. Since the initial color states are identical, the hadron multiplicity is predicted to be the same as in e^+e^- annihilation:

$$\langle n_{had}\rangle_{\ell p \to \ell' X} = n_{3\bar{3}}(W^2) = \langle n_{had}\rangle_{e^+e^- \to X}\Big|_{s=W^2} \tag{7.2}$$

again with possible corrections of order one from flavor effects. The difference between a "diquark" $|qq\rangle\ \bar{3}$ system and a single antiquark $\bar{3}$ should not be discernible in the central region where the rising multiplicity is created; only the total quantum number is relevant. Eq. (7.2) naturally predicts that there is no q^2 dependence of the multiplicity at fixed W^2, which is in agreement with the experimental results (Fig. 1).

It is interesting to contrast the color description of hadron multiplicity with the standard intuitive arguments of the parton model. Let us consider the multiplicity distribution for current-induced and hadron-induced collisions in the center-of-mass system. (See Section 3 and Fig. 9.) In deep inelastic scattering the final state consists of a hadron fragment with momentum $(1-x)p_H^z = -\frac{1}{2}W$ and a reversed quark of momentum $xp_H^z + q^z = \frac{1}{2}W$ which began as a quark at momentum $xp_H^z = -q^2/2W$. According to Bjorken,[3] Feynman,[20] and others, the multiplicity consists of two components: (a) the hadron-initiated multiplicity associated with the rapidity interval between the hadron fragment and the missing quark (or "hole") and (b) a quark-related multiplicity filling the gap between the hole and the final state quark. Thus

$$\langle n\rangle_{\ell p \to \ell' X} = C_{had} \log \frac{1-x}{x} + C_{e^+e^-} \log |q^2| \,. \tag{7.3}$$

In the hadronic collision case, the communicating parton has very low momentum, and we have two hadronic pieces so that

$$\langle n\rangle_{H_1 H_2 \to X} = C_{had} \log \frac{\sqrt{s}}{2} + C_{had} \log \frac{\sqrt{s}}{2} \,. \tag{7.4}$$

In general, it should be stressed that the hadronic and quark multiplicity mechanisms may be quite different (Fig. 20). The quark mechanism, being like that in

e^+e^- annihilation, must, by timing arguments,[3] be some kind of inside-outside cascade[43] or other vector gluon mechanism. The hadronic multiplicity, in contrast, is usually thought to arise from a multiperipheral chain initiated long before the actual collision. The multiplicity $<n>_{\ell p \to \ell' X}$ becomes a function solely of W^2 only if $C_{had} \equiv C_{e^+e^-}$ and the multiplicity is exactly proportional to a single power of logarithm.[46] In contrast, Eq. (7.2) is an immediate consequence of the color model, since in each case one has the identical timelike separation of the color currents.

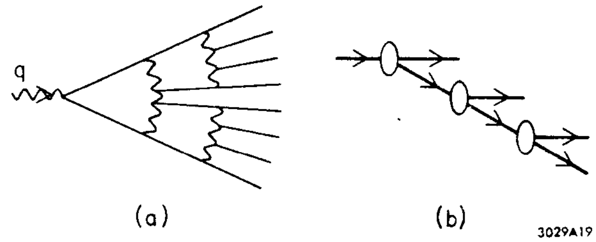

Fig. 20--(a) e^+e^- annihilation – the inside-outside cascade, and (b) the multiperipheral model.

Thus far our discussion for multiplicity in lepton-induced reactions has been limited to the region $x \gtrsim 0.2$, where the hadron can be represented in terms of its valence quarks. A crucial question is whether we can trust the result (7.2) as $\omega = x^{-1} \to \infty$ (or $q^2 \to 0$) where the $\bar{3}$ system becomes increasingly complicated. Implicit to this result is the presumption that the $\bar{3}$ system acts as a coherent state of limited mass. As $x \to 0$ ($\omega \to \infty$) it is usual to assume that one probes the portions of the proton's Fock space wave function with large numbers of quarks - each carrying a small fraction of the proton's total momentum. Nonetheless, prior to interaction all quarks have essentially the same velocity and the state mass is equal to the proton mass. The colliding current interacts with a quark of given momentum, but this need not affect the mass or coherence of the remaining core $\bar{3}$ system which then begins to radiate colored gluons. Dynamically some assumption such as strong binding may be needed to motivate this continued coherence.

In this picture hadron production in the central region only depends upon the total color, $\bar{3}$, of the core system, and "valence" effects are confined to the target fragmentation region. One consistency check for the applicability to the wee region can be considered. In $e^+e^- \to H + X$ with $z = 2p_H \cdot q/q^2$ ($q^2 = s$) the picture for large z is as shown in Fig. 18c. For large z the time between the creation of the quark and antiquark by the current and the emission of H is small. Thus additional hadron production occurs in the rapidity gap between the $\bar{3}$ with momentum $(1-z)\sqrt{s}/2$ and the 3 with momentum $\sqrt{s}/2$. Thus

$$\langle n \rangle_{e^+e^- \to HX} = n_{3\bar{3}}((1-z)s) = n_{3\bar{3}}(W^2) . \qquad (7.5)$$

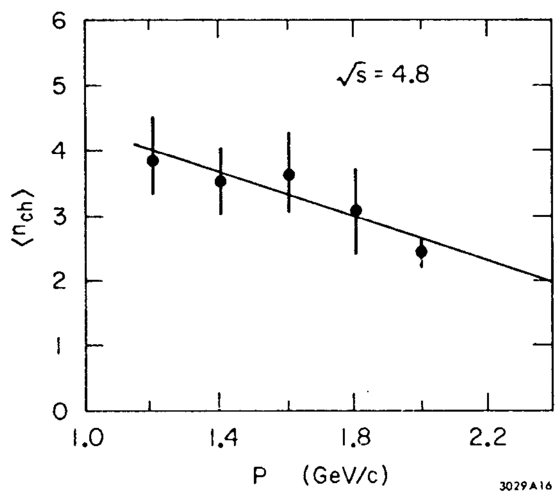

Fig. 21--The mean charged multiplicity in $e^+e^- \to \pi^\pm X$ as a function of pion momentum. (From Ref. 47.)

The predicted decrease of $\langle n \rangle$ with hadron momentum p_H is in fact supported experimentally[47] (see Fig. 21). We can now consider the continuation of this result to z = 0. Physically, the observation of a slow hadron should only affect the multiplicity by a number of order one. This is consistent with the $z \to 0$ limit of Eq. (7.5)

$$\langle n \rangle_{e^+e^- \to HX} \xrightarrow[z \to 0]{} n_{3\bar{3}}(s)$$
$$\sim \langle n \rangle_{e^+e^- \to X} - 1 \qquad (7.6)$$

Clearly, assigning extra multiplicity to the $\bar{3}$ system, as it becomes increasingly complicated as $z \to 0$, would lead to an inconsistency. This also suggests, by analogy, that the $x \to 0$ limit of the deep inelastic multiplicity (7.2) should be correct.

Eq. (7.2) has only been derived in the Bjorken scaling region of deep inelastic scattering. However, if we heuristically assume that the limits $x \to 0$ and $q^2 \to 0$ are equivalent, then we obtain $\langle n_{had} \rangle_{\gamma H \to X} = n_{3\bar{3}}(s)$, even for real photons. However, since real photon interactions are hadron-dominated, then evidently

$\langle n_{had}\rangle_{H_1H_2 \to X} = n_{3\bar{3}}(s)$, i.e., purely hadronic processes are described by the same universal multiplicity function. As we have noted in Section 2, this agrees with the phenomenological observations of Ref. 18, shown in Figs. 4-8.

Let us examine in more detail the question of whether the universality of multiplicity could in fact extend to purely hadronic reactions. We will see that such universality does not hold in all models. For instance, consider the color gluon multiplicity generated in the Low-Nussinov model[48] of the Pomeron, Figs. 22a,b. In this model the bare Pomeron corresponds to double color-gluon exchange in the elastic amplitude, and single color-octet gluon exchange in the case

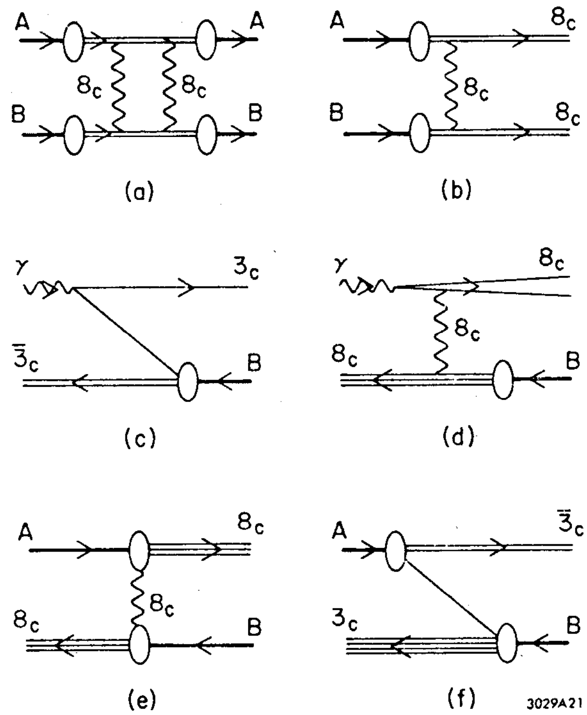

Fig. 22--(a) Bare Pomeron contribution to elastic scattering from gluon exchange in the Low-Nussinov model;[48] (b) contribution to inelastic production at the time of the first interaction, obtained from the absorptive part of (a); (c) quark exchange contribution to deep inelastic electron scattering; (d) color gluon exchange contribution to deep inelastic electron scattering; (e) color gluon exchange contribution to A+B→X; (f) quark exchange contribution to A+B →X.

of production processes. Thus in hadron-hadron collisions (Fig. 22e) the final state at the point of first interaction consists of separating octets of color. In lowest order, the gluon multiplicity from separating octets turns out to be 9/4 times the gluon multiplicity from 3 and $\bar{3}$. [More generally, in SU(n), this ratio is $2/(1-n^{-2})$.] Thus we would apparently expect $\langle n\rangle_{H_1H_2 \to X} \sim (9/4)\langle n\rangle_{e^+e^- \to X}$ at the same available energy, in apparent conflict with the available data. A more serious difficulty is that as $x \to 0$ in deep inelastic scattering the Pomeron gluon exchange graph of the Low-Nussinov model (Fig. 22d) should be dominant over the quark exchange graph (Fig. 22c), so that at fixed W^2 the multiplicity would be expected to rise by approximately a factor of two as the wee x region is approached. It may be possible to avoid these conflicts with the data if there are strong corrections from higher order perturbation theory or if the monotonic relationship of hadron to gluon multiplicity is incorrect. The evaluation of the dependence of hadron multiplicity in the Low-Nussinov model is an important empirical and theoretical question.

In the case of dual models similar difficulties may arise. Typically, the Huan Lee-Veneziano[49] approach suggests that for every planar Reggeon type of diagram contributing to n particle production in hadron-hadron scattering there are 2^n as many nonplanar diagrams which go into building up the Pomeron. Thus if we could "turn off" the nonplanar contributions the average multiplicity would change from $\langle n\rangle \propto 2g^2$ to $\langle n\rangle \propto g^2$. This is precisely what we should be able to do in deep inelastic scattering by varying x. At small x nonplanar diagrams certainly contribute in the dual approach, but, as $x \to 1$, the valence planar topologies would be expected to take over. Thus it may be very difficult for this type of approach to be consistent with the q^2 and x-independence of $\langle n\rangle_{\ell p \to \ell X}$ displayed in Fig. 1.

We can, however, construct a simple model in which universality for multiplicities in lepton- and hadron-induced collisions is immediately evident. Thus let us suppose that the initial interaction between the incoming hadrons in a production process is simply $\bar{3}$ or 3 exchange as in Fig. 22f. This is essentially the wee-parton exchange model of Feynman,[20] where we have assumed that the parton is a wee quark. Equivalently, the interaction could be the annihilation of a slow quark and antiquark (or qq system) to make a slow hadron (i.e., $q+q \to M$ or $q+qq \to B$) in the central region. Assuming that the spectator systems continuing in the beam and target directions radiate as coherent systems, we again have a separating $3, \bar{3}$ color system and universal multiplicity:

$$\langle n \rangle_{H_1 H_2 \to X} = n_{3\bar{3}}(s) = \langle n \rangle_{e^+e^- \to X} . \qquad (7.7)$$

We emphasize how different this underlying physical picture of color separation is from the multiperipheral model. In the color models, the incoming hadrons do not radiate and the multiplicity is generated after the initial interaction from the timelike current separation. In contrast, the multiperipheral model requires that most of the multiplicity is generated prior to the actual collision. Thus in the color model the multiplicity "jet" axis will not always be the same as the beam axis while in the usual hadronic models the multiplicity axis would be expected to correspond more and more closely to the beam direction as s increases. None-theless, our approach preserves short range correlations in flavor quantum numbers since the only long range effects are color related. Further tests which can discriminate the quarklike nature of the hadronic jets will be discussed in Sections 10, 11, and 12.

Finally we note that, as for $e^+e^- \to HX$, the multiplicity for $H_1H_2 \to HX$ is given by the usual universal function: $\langle n \rangle_{H_1H_2 \to HX} = n_{3\bar{3}}(\mathcal{M}_X^2)$. We also expect that clustering effects, $\langle p_T \rangle$, etc., in the central "plateau" region will be the same for the jets in all lepton- and hadron-induced reactions.

8. GLUON MULTIPLICITY IN QED AND QCD

The predictions discussed in Section 7 are all independent of the exact functional dependence of the multiplicity $n_{3\bar{3}}(s)$. However, if we assume that the infrared behavior of the gluon bremsstrahlung in the color theory is similar to that of QED, then further results for the multiplicity and jet structure in the central region can be calculated in analogy with soft photon emission in electrodynamics. In QED, the production cross section for soft photons obeys a Poisson distribution,[50]

$$\sigma_n = \frac{(2\alpha\tilde{B})^n}{n!} e^{-2\alpha B} \sigma_0 \qquad (8.1)$$

$$\langle n_\gamma \rangle = 2\alpha \widetilde{B}\,(k_{max}) \tag{8.2}$$

where

$$2\alpha \widetilde{B}(k_{max}) = -\sum_{i,j} \frac{\alpha}{4\pi^2} Q_i Q_j \eta_i \eta_j \int_{k_{min}}^{k_{max}} \frac{d^3k}{k} \frac{p_i \cdot p_j}{p_i \cdot k p_j \cdot k} \;. \tag{8.3}$$

The sum is over all external charged particle pairs where $\eta_i = +1$ (-1) for an outgoing (ingoing) line. The photon angular integral is singular along the charged particle direction and one obtains

$$\langle n_\gamma \rangle = -\sum_{i,j} \frac{\alpha}{2\pi} Q_i Q_j \eta_i \eta_j \frac{1}{\beta_{ij}} \log \frac{1+\beta_{ij}}{1-\beta_{ij}} \int_{k_{min}}^{k_{max}} \frac{dk}{k} \tag{8.4}$$

where

$$\beta_{ij} = [1 - p_i^2 p_j^2/(p_i \cdot p_j)^2]^{\frac{1}{2}} \tag{8.5}$$

is the relative velocity for each pair and

$$y_{ij} = \tfrac{1}{2} \log \frac{1 + \beta_{ij}}{1 - \beta_{ij}} \tag{8.6}$$

is the relative rapidity. Thus the rapidity plateau arises naturally from the singularity of the angular integral, and the dk/k singularity serves to modify the height of this plateau. For an oppositely charged final state pair, we have

$$\langle n_\gamma \rangle = \begin{cases} \dfrac{2\alpha}{\pi} \left(\log \dfrac{s}{m^2} - 1\right) \log \dfrac{k_{max}}{k_{min}} \,, & s >> m^2 \\[2ex] \dfrac{4\alpha}{\pi} \; \dfrac{s-4m^2}{m^2} \log \dfrac{k_{max}}{k_{min}} \,, & s \sim \text{threshold} \end{cases} \tag{8.7}$$

If we take $k_{max} \sim \sqrt{s}/\langle n_\gamma \rangle$, then

$$\langle n_\gamma \rangle \sim \frac{\alpha}{\pi} \log \frac{s}{m^2} \log \frac{s}{k_{min}^2} \tag{8.8}$$

which for finite k_{min} gives a rising plateau.

In extending these results to QCD, the soft gluon multiplicity depends on the group theoretical constant calculated from the lowest order diagram if we can assume Poisson exponentiation as in Eq. (8.1). The only changes in the QED formulas are then

(a) The charge factor α is replaced by $\frac{4}{3}\alpha_s$, where $\alpha_s = g^2/4\pi$, g being the quark quark colored gluon coupling constant defined by

$$\mathscr{L}_{int} = g\bar{\psi}\gamma_\mu \lambda_a \psi A^a_\mu \ , \ \mathrm{Tr}\ \lambda_a^2 = 2 \tag{8.9}$$

(b) There is a natural infrared cutoff. For wavelengths longer than the confinement region of a typical hadronic size, a gluon can "see" only color singlet states and it thus decouples; therefore quark confinement leads to a cutoff,

$$k_{min} \sim \frac{1}{R_{conf}} \sim 0(m_{hadron}) \ , \tag{8.10}$$

and

$$\langle n_g \rangle \cong \frac{4}{3}\frac{\alpha_s}{\pi} \log \frac{s}{m_3 m_{\bar{3}}} \log \frac{s}{m^2_{hadron}} \tag{8.11}$$

Comparing to the $\log^2 s$ term in the fit of Albini et al.[18] to pp multiplicity, Eq. (2.3), and assuming

$$\frac{2}{3}\langle n_{had}\rangle = \langle n_{ch}\rangle \ , \ \langle n_{had}\rangle \cong \langle n_{gluon}\rangle \tag{8.12}$$

we obtain $\alpha_s \cong 0.47$, which indicates the typical size of the couplings involved.

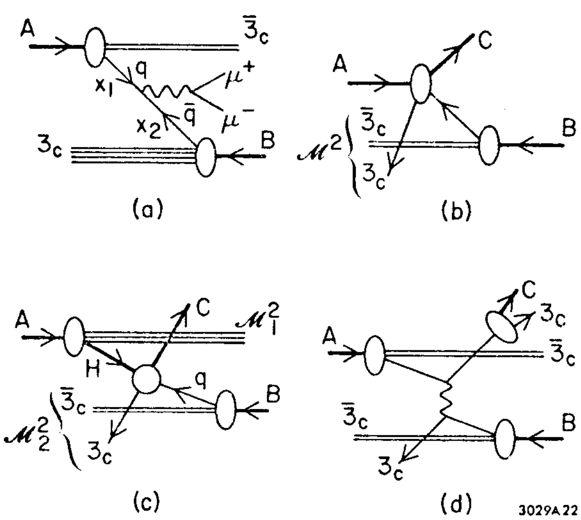

Fig. 23--Initial color current separation in (a) $AB \to \mu^+\mu^- X$, and (b)-(d) $AB \to C+X$ at large p_T. The important large angle subprocesses are (a) $q\bar{q} \to \mu^+\mu^-$, (b) $Aq \to Bq$, (c) $Hq \to Cq$, (d) $qq \to qq$.

9. HADRON MULTIPLICITY FOR HIGH p_T PROCESSES

There are a number of additional applications of the 3-$\bar{3}$ multiplicity picture.[51] In the Drell-Yan model for $pp \to \mu^+\mu^- X$ (Fig. 23a), the final state consists again of a rapidly separating

3 and $\bar{3}$ and we have

$$\langle n \rangle_{pp \to \mu^+\mu^- X} = n_{3\bar{3}}(\mathcal{M}^2) \tag{9.1}$$

where $\mathcal{M}^2 = (1-x_1)(1-x_2)s$ and x_1 and x_2 are the annihilating quark momenta fractions, obeying the usual constraints $x_1 x_2 s = \mathcal{M}^2$ and $x_1 - x_2 = x_F(\mu^+\mu^-)$.

Applications to high p_T processes should prove particularly fruitful. Four important subprocesses for $A+B \to C+X$ are illustrated in Fig. 23.

(a) The <u>fusion</u> process[15] $q\bar{q} \to H\bar{H}$ is analogous to the Drell-Yan process in color so that

$$\langle n \rangle = n_{3\bar{3}}(\mathcal{M}^2) \tag{9.2}$$

where

$$\mathcal{M}^2 \doteq (1-x_1)(1-x_2)s \ .$$

Of course, in the case where only one meson is triggered, an appropriate average over the accessible x_1 and x_2 values is to be performed. Since x_1 and x_2 are of order $x_T = 2p_T/\sqrt{s}$, $\langle n \rangle$ tends to decrease with increasing p_T at fixed s, in contradiction to experiment.[7,8,13]

(b) The <u>leading particle diagram</u>[52] of Fig. 23b has an easily computed multiplicity arising from the indicated 3 and $\bar{3}$ color separation. We predict

$$\langle n \rangle = n_{3\bar{3}}(\mathcal{M}^2) \tag{9.3}$$

where in this case $\mathcal{M}^2 = (1-x_T)s$. Again $\langle n \rangle$ is predicted to decrease with increasing p_T at fixed s.

(c) The <u>$qM' \to qM$</u> scattering subprocess[53] yields two contributions to the hadron multiplicity: the first component arises due to the emission of the daughter meson M' from the incoming proton (which requires internally a separated 3 and $\bar{3}$ of color whose rapidity separation we denote by $\mathcal{M}_1^2$ in Fig. 23c); the second is that due to the explicit separation of the 3 and $\bar{3}$ in color corresponding to $\mathcal{M}_2^2$.

Here

$$\mathcal{M}_2^2 = z(s+t)+u \cong \frac{x_T}{2}(1-x_T)s$$

and (9.4)

$$\mathcal{M}_1^2 = 0(m^2)/z \cong 0(m^2)/x_T ,$$

where we used the fact that z on the average is of order x_T. The behavior of the net multiplicity here is close to the experimental trend, remaining roughly constant, and even increasing slightly with p_T at low trigger momentum.

(d) All the above processes are very different from the final case $qq \to qq$ scattering[54] (Fig. 23d). The multiplicity here has several contributions which will be discussed in detail elsewhere.[51] Note however that double neutralization is required in the final state, since there are two 3-$\bar{3}$ separated pairs. The predicted multiplicity is correspondingly large, in fact too large for consistency with the data, if we normalize relative to $\langle n\rangle_{e^+e^-}$. This is a reflection of the fact that this diagram connects smoothly in the exclusive limit to the Low-Nussinov Pomeron model[48] which, as we have already indicated, predicts approximately twice the desired multiplicity for hadron-hadron collisions.

Thus, color gluon emission provides a predictive framework for describing hadron production, leading to an interpretation of universal multiplicity, and why "plateau" regions should have the same features for all processes. However, we have still to discuss possible interesting effects in the fragmentation regions appropriate to various processes. We will see that this provides additional support for the color model.

10. JET FRAGMENTATION IN HADRON-INDUCED REACTIONS

The fragmentation region in hadron-induced reactions may prove to be one of the most important tools in unraveling the underlying structure of hadronic jets. It is worth emphasizing that the usual triple Regge expansion does not appear to be applicable to ISR data. The standard Regge prediction for $pp \to \pi^+X$ as $x \to 1$ is $d\sigma/dx\, dt \sim (1-x)^F \beta(t)$, where the power F depends on the exchanged baryon

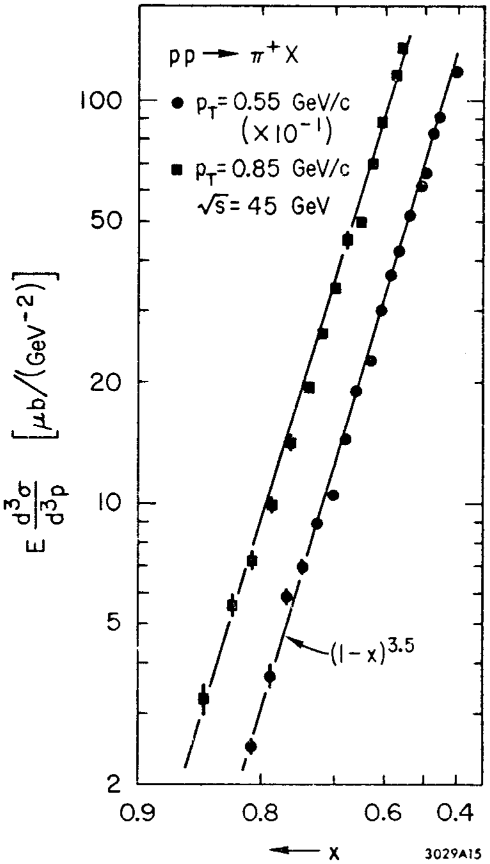

Fig. 24--ISR data for $pp \to \pi^+X$. The figure is from Ref. 55.

trajectory, $F = 1\text{-}2\alpha(t)$. This implies that F should vary with t and be close to zero at small t. In fact, experimentally, $F \sim 3.5$ <u>independent</u> of $|t| \sim p_T^2$. This is shown graphically in Ochs' plot[55] of the ISR data[56] (see Fig. 24).

Fixed powers are in fact exactly what is predicted (see Ref. 57) for parton models. We will discuss the detailed predictions for the powers and comparisons with experiment in the next section. First, however, following Ochs,[55] let us consider the π^+/π^- ratio in the proton fragmentation region. Since the $x \to 1$ power behavior of $d\sigma/dx$ $(pp \to \pi X)$ is so close to that observed for $\nu W_2^p(x)$ at SLAC, one can speculate that these pions are the direct fragments of the quarks in the proton. Assuming $D_{\pi^+/u} >> D_{\pi^+/d}$, Ochs then predicts at large x

$$R(\pi^+/\pi^-) \equiv \frac{d\sigma/dx(pp \to \pi^+X)}{d\sigma/dx(pp \to \pi^-X)} = \frac{G_{u/p}(x)}{G_{d/p}(x)} \tag{10.1}$$

i.e.,

$$\frac{\nu W_2^{en}}{\nu W_2^{ep}} = \frac{4 + R(\pi^+/\pi^-)}{4\,R(\pi^+/\pi^-)+1} . \tag{10.2}$$

This relationship is quite well satisfied over the entire range of x, as shown in Fig. 25. [Recall, however, that there are large uncertainties in the neutron structure function for x > 0.8.] In fact, the experimental approach of $R(\pi^+/\pi^-)$ to 5 at $x \to 1$ leads to the prediction $\nu W_2^{en}/\nu W_2^{ep} \to 3/7$, the value predicted by Farrar and Jackson.[58] Away from x near 1 the above analysis will be somewhat modified if a finite $D_{\pi^+/u}/D_{\pi^-/u}$ is used, as determined, for example, by the $\nu p \to \mu^- X$ data.[27] This procedure will also allow for the effects of resonance production and decay, especially $\rho^0 \to \pi^+\pi^-$.

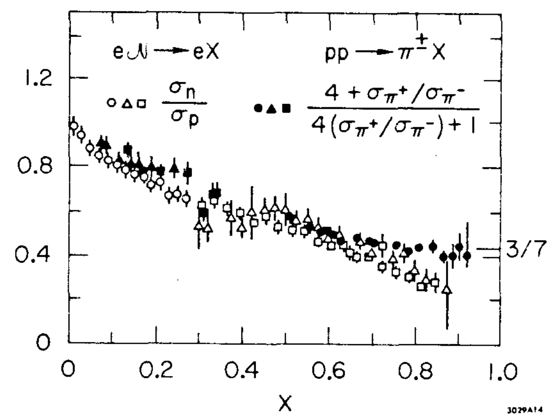

Fig. 25--Ochs' comparison of the neutron-proton ratio in deep inelastic scattering, and inclusive $\pi^\pm$ production. The functions should be the same if the π^+/π^- ratio follows the u/d quark ratio in the proton, as in Eq. (10.2). (From Ref. 55.)

11. QUARK COUNTING RULES FOR FRAGMENTATION DISTRIBUTIONS

There are several interesting empirical observations that seem to indicate that hadronic and quark jets are closely related:

(a) The fact discussed in Section 10 that the power F in hadron fragmentation $d\sigma/dx\, dp_T^2 \sim (1-x)^F$ at $x \sim 1$ is independent of momentum transfer at low p_T.

(b) The indication that the π^+/π^- ratio follows the u/d quark ratio in the proton, as was seen in Fig. 25.

(c) The fact that the particle ratios π^+/π^- and K^+/K^- (although not $\bar{p}/p$) have the same behavior as $(1-x) \to 0$ in the beam direction and as $(1-x_T) \to 0$ at 90° in large p_T reactions. The importance of these features has been particularly emphasized by Ochs.[53]

In order to explore this phenomenology more quantitatively, it is useful to have model predictions for the power dependence of the jet fragmentation functions $G_{A/H}(x)$. Here H and A represent quark or hadronic systems. In the simplest model one assumes limited high momentum components in the bound state wave function (finite Bethe-Salpeter wave functions at $x^\mu \to 0$), and then iterates the kernel wherever large relative momentum is required. The power behavior is then easily computed from Born graphs in renormalizable perturbation theory, and is found to depend only on the number of constituent fields in the spectator system $A + \bar{H}$. Thus if A is a fragment of H with $x = \left(p_A^o + p_A^z\right)/\left(p_H^o + p_H^z\right)$ ($\rightarrow |\vec{p}_A|/|\vec{p}_H|$ at infinite momentum), then one predicts[58,59]

$$G_{A/H}(x) \sim (1-x)^{2n_s-1} \qquad (x \rightarrow 1) \tag{11.1}$$

where n_s is the number of spectator quarks left behind. The power dependence reflects the reduction of available phase space due to the spectators. The rule also gives a smooth exclusive-inclusive connection with the dimensional counting rules for exclusive processes. [Technically, if A+H is a fermion system, there is an extra power of (1-x) spin suppression in $G_{A/H}$.[59] However, as has been shown in $e^+e^- \rightarrow HX$, nonscaling contributions negate this suppression at $\mathcal{M}^2/s \rightarrow 0$;[60] for simplicity, we shall retain the rule (11.1) here for all spins.] Specific examples of Eq. (11.1) are $\nu W_2^{ep} \sim G_{q/p} \sim (1-x)^3$, $G_{\bar{q}/p} \sim (1-x)^7$, $G_{\pi/p} \sim G_{K^+/p} \sim (1-x)^5$, $G_{\pi/q}(x) = D_{\pi/q}(x) \sim 1-x$, $G_{K^-/p} \sim (1-x)^9$, $G_{\bar{p}/p} \sim (1-x)^{11}$. The prediction for $G_{\bar{q}/p}$ appears to be consistent with the present experimental parametrizations for the antiquark distributions in the Drell-Yan process $pp \rightarrow \mu^+\mu^- X$. A further prediction for the forward fragmentation region is

$$\frac{d\sigma/dx\ (pp \rightarrow \psi X)}{d\sigma/dx\ (\pi p \rightarrow \psi X)} \sim (1-x)^2\ ,\ x \rightarrow 1 \tag{11.2}$$

because of the extra quark spectator.

The dimensional counting rules can also be tested in deuteron reactions. The predictions[61] are

$$\frac{d\sigma}{dx\, dq^2}(eD \rightarrow epn) \sim \frac{4\pi\alpha^2}{q^4} F_p^2(q^2) G_{p/D}(x) \tag{11.3}$$

for deuteron breakup in electroproduction, and[61,62]

$$\frac{d\sigma/dx\ (Dp \rightarrow \pi X)}{d\sigma/dx\ (pp \rightarrow \pi X)} \sim (1-x) G_{p/D}(x) \tag{11.4}$$

for inclusive meson production at $x \rightarrow 1$. Both predictions seem to provide successful parametrizations of the data using $G_{P/D}(x) \sim (1-x)^5$, ($n_s = 3$).

The threshold behavior for $G_{P/D}(x)$ at $x \sim 1$ is related by the exclusive-inclusive connection to the dimensional counting prediction $(q^2)^5 F_D(q^2) \rightarrow$ const[33] for the dueteron form factor. The data at lower q^2 can be compared with the prediction $(q^2-m_0^2)f_D(q^2) \rightarrow$ const[63,61] where the "reduced" form factor $f_D(q^2) \equiv F_D(q^2)/F_N^2(q^2/4)$ has the effect of the falloff of the baryon form factors removed. The comparison with experiment[64] is shown in Fig. 26.

Nuclear targets also allow a number of intriguing tests of the quark parton model and jet structure.[65] For example, the observation of electroproduction of hadrons in a nuclear target will allow the study of quark jet propagation through hadron matter. There are a number of tests of the hypothesis that wee quarks are shadowed; this can be tested in detail in the Drell-Yan process for nuclear targets.[66]

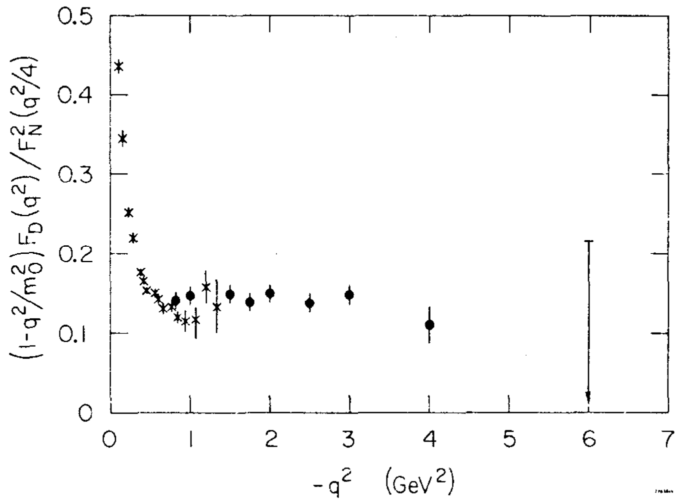

Fig. 26--The reduced deuteron form factor $f_D(q^2)$ measured in Ref. 64 multiplied by $1-q^2/m_0^2$, with $m_0^2 = 0.24$ GeV^2. Quark counting predicts this curve approaches a constant. (From Ref. 61.)

If hard partons are not shadowed, then quasi-elastic large angle scattering (without inelastic hadron production) should obey the impulse approximation: in particular, in the constituent interchange model $K^+A \rightarrow K^+A'$ only depends on the number of up quarks in the nuclear target.[67] We also note that absence of shadowing enhances the counting rate and increases the possibility of observing very high p_T exclusive processes on a nucleon target. Further consequences of the parton model for nuclear reactions are discussed in Refs. 66 and 67.

We also wish to emphasize the importance of testing the dimensional counting scaling laws for multiparticle exclusive channels in e^+e^- annihilation. The predicted cross section behavior maintaining fixed angle between all observed particles is[33]

$$\sigma(s) \sim s^{-(1+N_M+2N_B)} \quad , \quad s \to \infty \tag{11.5}$$

where N_M and N_B are the number of mesons and baryons in the final state. Some recent proofs of dimensional counting for form factors and large angle scattering in various models are given in Refs. 68 and 69.

12. FRAGMENTATION MODELS FOR HADRON COLLISIONS

As we have noted in Section 11, the p_T-independence of the x near one behavior of the forward fragmentation cross section in hadron collisions suggests that these distributions are related to the jet fragmentation functions $G_{A/B}(x)$. The quark-counting rules (11.1) allow us to differentiate the various possible models for the fragmenting jet.

There are two distinct models for the jet structure of hadron-induced reactions which we shall consider here.

(1) The fragmentation distribution for $A + B \to H + X$ at $x \to 1$ is given by $G_{H/A}$ $G_{H/A}(x)$; this is natural in models where H is formed in the diffractive dissociation of the beam particle[57] (see Fig. 27a). The same predictions are also obtained in the Low-Nussinov gluon-exchange model.

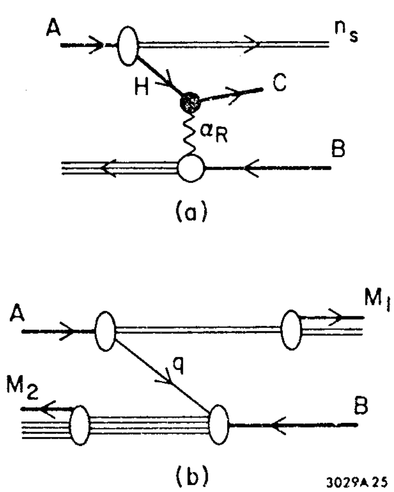

Fig. 27--(a) Diffractive dissociation contribution to the forward inclusive cross section $A + B \to C + X$. (b) Quark exchange contribution to $A + B \to M_1 + X$ and $A + B \to M_1 + M_2 + X$.

(2) If the initial interaction is caused by wee quark exchange,[20,19,51] or by processes such as slow quark-antiquark annihilation, then the spectator system in baryon-baryon collisions is a $\bar{3}$ in SU(3) color and contains at least two quarks (see Fig. 27b). The corresponding system moving in the other direction is a qqqq state. Such configurations in color lead to universal hadron multiplicity as discussed in Section 7. In the case of meson-baryon collisions, the minimal system in the meson fragmentation region is a quark jet, with a qq jet moving in the opposite direction. Thus in this model the fragmentation region for $A + B \to H + X$ depends on $G_{A/q}$, $G_{A/qq}$, $G_{A/qqqq}$, etc.

It should be emphasized that the fragmentation of qq and qqqq jets can already be studied in the target fragmentation region in deep inelastic lepton scattering and the proton fragmentation region in the Drell-Yan process $pp \to \mu^+\mu^- X$.

Models (1) and (2) give identical predictions for the ratio of particle distributions. For example, the counting rule (11.1) predicts

$$R(K^-/K^+) = d\sigma/dx[pp \to K^- X]/d\sigma/dx[pp \to K^+ X] \sim (1-x)^4 \text{ for } x \to 1 \tag{12.1}$$

because there are two additional spectators. Experimentally, the ISR data ($p_T \sim$ 0.6 GeV, $x < 0.8$) indicates $R_{exp}(K^-/K^+) \sim (1-x)^3$. The ISR data also gives $R_{exp}(\bar{p}/p) \sim (1-x)^{13}$ for $p_T \sim 0.4$ GeV, $x < 0.3$. The $x \to 1$ rule is clearly not reliable in this range, but the asymptotic prediction is $R(\bar{p}/p) \sim (1-x)^{12}$. We also predict $R(\pi^+/\pi^-) \to C > 1$. The qualitative features of the data seem to be obtained in this jet fragmentation approach, although much more data, especially using meson and photon beams, is needed.

The absolute power of the fragmentation distribution at $x \to 1$ can be used to differentiate between models. Thus for $pp \to \pi^+ X$, $K^+ X$ we predict

$$d\sigma/dx \sim \begin{cases} D_{\pi^+/qqq}(x) \sim (1-x)^5 \\ D_{\pi^+/qq}(x) \sim (1-x)^3 \end{cases} \tag{12.2}$$

for models (1) and (2) respectively. The data indicates $d\sigma/dx(pp \to \pi^+X) \sim (1-x)^{3.5}$, thus favoring the model based on quark exchange and universal multiplicity. There are, however, several points which could complicate this analysis, since the predictions can be modified by spin effects, nonleading terms from resonance decay, and Reggeon exchange plus fragmentation contributions as indicated in Fig. 27a.

13. CONCLUSION

One of the most exciting aspects of the phenomenology of jet production is the hint that we are studying basic (virtual) quark processes - even in hadron-induced reactions. If the suggestions of current theoretical models[19,44,48,53,57] are correct, as we have discussed here, then there can be a unified description of lepton and hadron-induced reactions at both large and small transverse momentum in terms of an underlying quark dynamics. Further experimental work, especially the comparison of multiparticle processes for different beams - photons, leptons, mesons, and baryons - will be required in order to discriminate and classify the various types of quark-jet, multiquark-jet, and hadron-jet candidates. We have also emphasized the utility of a number of different phenomenological tools, including quantum number retention tests, fragmentation power laws, as well as multiplicity and momentum distributions and scaling tests, which can probe the underlying jet structure.

ACKNOWLEDGEMENTS

We wish to thank J. Bjorken, R. Blankenbecler, H. Miettinen, H. Kühn, L. Stodolsky, and W. Ochs for helpful comments. We are also grateful to Professor W. Zimmerman and L. Stodolsky for the warm hospitality of the Max Planck Institute, where this talk was prepared.

REFERENCES

1. G. Hanson et al., SLAC-LBL collaboration, these proceedings; and Phys. Rev. Letters 35, 1609 (1975).

2. G. Wolf, International Symposium on Lepton and Photon Interactions at High Energies, Stanford, 1975; P. H. Gabrincius et al., Phys. Rev. Letters 32, 328 (1974); A. J. Sadoff et al., Phys. Rev. Letters 32, 955 (1974). See also C. del Papa et al., SLAC-PUB-1708 (1976), and C. Heusch, these proceedings.

3. J. Bjorken and J. Kogut, Phys. Rev. D8, 1341 (1973); J. D. Bjorken, Proceedings of the Summer Institute on Particle Physics, edited by M. Zipf, SLAC-167 (1973); J. D. Bjorken, SLAC-PUB-1756 (1976).

4. See R. Dashen, International Symposium on Lepton and Photon Interactions at High Energies, Stanford (1975), and references therein.

5. F. J. Gilman, International Symposium on Lepton and Photon Interactions at High Energies, Stanford (1975), and references therein.

6. See reports of R. F. Mozley, L. Mo, K. M. Hanson, V. Eckardt, and G. Wolf in the Proceedings of the International Symposium on Lepton and Photon Interactions at High Energies, Stanford (1975), and C. Heusch, these proceedings.

7. P. Darriulat et al., Nucl. Phys. B107, 429 (1976). For reviews see M. Della Negra, these proceedings and P. Darriulat, XVII International Conference on High Energy Physics, Tbilisi (1976).

8. CERN-College de France, Heidelberg-Karlsruhe (CCHK) collaboration. M. Della Negra et al., Nucl. Phys. B104, 365 (1976), and M. Della Negra, Ref. 7.

9. D. Sivers, S. J. Brodsky, and R. Blankenbecler, Physics Reports 23C, 1 (1976).

10. R. Blankenbecler, S. J. Brodsky, and J. F. Gunion, Phys. Letters 39B, 649 (1972); Phys. Rev. D6, 2652 (1972); Phys. Letters 42B, 461 (1973); Phys. Rev. D8, 287 (1973); Phys. Rev. D12, 3469 (1975). A recent comparison of the CIM with experiment is given by J. Gunion and S. Brodsky, these proceedings and SLAC-PUB-1806 (1976).

11. See P. Darriulat et al., Ref. 7, the reviews of P. Landshoff, M. Della Negra, R. Field, these proceedings, and R. Baier et al., University of Bielefeld (1976).

12. K. Eggert et al., Nucl. Phys. B98, 73 (1975); G. Finocchiaro et al., Phys. Letters 50B, 396 (1974); see also Ref. 7.

13. R. D. Kephart, Stony Brook University Thesis (1975); Pisa-Stony Brook collaboration, G. Finocchiaro et al., Phys. Letters 50B, 396 (1974); R. Castaldi, presented at the Xth Rencontre de Moriond, Meribel, France (1975).

14. S. J. Brodsky and G. Farrar, Phys. Rev. Letters 31, 1153 (1973) and Phys. Rev. D11, 1304 (1975); V. A. Matveev, R. M. Muradyan, and A. N. Tavkhelidze, Nuovo Cimento Letters 7, 719 (1973). For recent reviews see D. Sivers et al., Ref. 9, and S. J. Brodsky in the proceedings of the SLAC summer Institute on Particle Physics, SLAC-191, November (1975) and SLAC-PUB-1733.

15. P. V. Landshoff and J. C. Polkinghorne, Phys. Rev. D8, 4157 (1973), Phys. Rev. D10, 891 (1974), and references therein. See also G. Preparata and M. Rossi, CERN preprint (1976).

16. For a different view, see P. V. Landshoff, these proceedings.

17. For a review and references, see R. Stroynowski, Sixth International Colloquium on Multiparticle Reactions, Oxford (1975).

18. E. Albini et al., Nuovo Cimento 32A, 101 (1976), and references therein.

19. S. Brodsky and J. F. Gunion, Phys. Rev. Letters 37, 402 (1976).

20. R. P. Feynman, Photon-Hadron Interactions, (W. A. Benjamin, New York, 1972); Phys. Rev. Letters 23, 1415 (1969).

21. G. Farrar and J. Rosner, Phys. Rev. D7, 2747 (1973). R. Cahn and E. Colglazier, Phys. Rev. D9, 2658 (1974).

22. J. Vander Velde, presented at the IVth International Winter Meeting on Fundamental Physics, Salardu, Spain (1976); University of Michigan preprint. A. Seidl, these proceedings.

23. J. Bjorken, Ref. 3; R. Feynman, Ref. 20; see also Ref. 21.

24. R. Feynman, Ref. 20; J. Dakin and G. Feldman, Phys. Rev. D8, 2862 (1973).

25. J. Gunion, Phys. Rev. D11, 1796 (1975).

26. J. F. Martin, private communication, and J. F. Martin et al., SLAC-PUB-1766 (1976).

27. J. Bjorken and H. I. Miettinen, private communication.

28. J. Bjorken and E. Paschos, Phys. Rev. D1, 1450 (1970).

29. S. J. Brodsky, J. F. Gunion, and R. L. Jaffe, Phys. Rev. D6, 2488 (1972).

30. S. J. Brodsky, F. E. Close, and J. Gunion, Phys. Rev. D5, 1384 (1972); Phys. Rev. D6, 177 (1972); Phys. Rev. D8, 3678 (1972).

31. S. Brodsky and G. Farrar, Ref. 14.

32. R. L. Anderson et al., Phys. Rev. D14, 679 (1976).

33. S. Brodsky and G. Farrar, Ref. 14.

34. G. R. Farrar and S. C. Frautschi, Phys. Rev. Letters 36, 1017 (1976).

35. A. Eisner et al., Phys. Rev. Letters 33, 865 (1974), and UC-Santa Barbara preprint, presented to the Bonn Conference (1973).

36. S. J. Brodsky, C. Carlson, and R. Suaya, SLAC-PUB-1791 (to be published in Phys. Rev.).

37. The effect of color on inelastic compton scattering is discussed by M. Chanowitz, LBL-5312 (1976) and LBL-4237 (1975).

38. A. Boyarski et al., SLAC-PUB-1694 (1975).

39. We would like to thank H. Miettinen for helpful discussions on this topic.

40. R. Blankenbecler and S. Brodsky, Phys. Rev. D10, 2973 (1974); J. F. Gunion, Phys. Rev. 10, 242 (1974). R. Blankenbecler, J. F. Gunion, and S. J. Brodsky, Phys. Rev. D12, 3469 (1975). See also S. Brodsky, in the proceedings of the SLAC Summer Institute in Particle Physics (1974).

41. S. J. Brodsky (to be published).

42. We wish to thank K. Gaemers for discussions on this topic.

43. J. Kogut, D. Sinclair, and L. Susskind, Phys. Rev. D7, 3637 (1973). See also J. Bjorken, Ref. 3, and N. Craigie, A. Kraemmer, and K. Rothe, Z. Phys. 259, 1 (1973).

44. L. Stodolsky, Phys. Rev. Letters 28, 60 (1972). See also the jet models of G. Preparata, Proceedings of the International School of Sub-Nuclear Physics, Erice (1974); H. Satz, these proceedings; K. Kinoshita, University of Bielefeld preprint (1976); and W. Morton, DAMTP preprint (1976), and references therein.

45. SLAC-LBL collaboration (unpublished). We thank R. Schwitters for communicating this result to us.

46. J. Bjorken and J. Kogut, Ref. 3, argue that consistency with the Regge behavior of exclusive electroproduction processes requires $C_{e^+e^-} = C_{had}$.

47. B. A. Barnett, Maryland-Pavia-Princeton collaboration, presented at the Second International Conference on High Energy Physics, Vanderbilt University (1976).

48. F. E. Low, Phys. Rev. D12, 163 (1975); S. Nussinov, Phys. Rev. Letters 34, 1286 (1973), and IAS preprint COO-2220-57 (1975).

49. H. Lee, Phys. Rev. Letters 30, 719 (1973); G. Veneziano, Phys. Letters 43B, 413 (1973). We wish to thank H. I. Miettinen for helpful conversations concerning this model.

50. D. R. Yennie, S. C. Frautschi, and H. Suura, Annals of Physics 13, 379 (1961). D. R. Yennie, Brandeis Summer Lectures in Theoretical Physics, Vol. I (1963). S. Weinberg, Phys. Rev. 140, B516 (1965).

51. S. J. Brodsky and J. F. Gunion, to be published.

52. R. Blankenbecler, S. Brodsky, and J. Gunion, Phys. Rev. D6, 2652 (1972); P. Landshoff and J. Polkinghorne, Ref. 15.

53. R. Blankenbecler, S. Brodsky, and J. Gunion, Phys. Letters 42B, 461 (1972).

54. S. Berman, J. Bjorken, and J. Kogut, Phys. Rev. D4, 3388 (1971).

55. W. Ochs, Cal-Tech preprint 68-542 (1976).

56. Bonn-Hamburg-Munich collaboration, V. Blobel et al., Nucl. Phys. B69, 454 (1974).

57. R. Blankenbecler and S. Brodsky, Ref. 40. See also H. Goldberg, Nucl. Phys. B44, 149 (1972).

58. J. F. Gunion, Ref. 40. See also S. Brodsky and G. Farrar, Ref. 14.

59. F. Ezawa, Nuovo Cimento 23A, 271 (1974). See also D. Sivers et al., Ref. 9.

60. G. R. Farrar and D. R. Jackson, Phys. Rev. Letters 35, 1416 (1975).

61. S. Brodsky and B. Chertok, Phys. Rev. Letters 37, 269 (1976); SLAC-PUB-1759, to be published in Phys. Rev.

62. E. Lehman, Phys. Letters 62B, 296 (1976).

63. S. Brodsky, in the Proceedings of the International Conference on the Few Body Problem, Quebec (1974).

64. R. Arnold et al., Phys. Rev. Letters 35, 776 (1975).

65. See W. Busza, these proceedings.

66. The application of the parton model to nuclear distributions and shadowing is discussed in J. Kühn, S. Brodsky, and J. Gunion (to be published), and J. Kühn, these proceedings.

67. S. Brodsky and J. Kühn (to be published). We would like to thank D. R. Yennie for discussions on this topic.

68. M. Goldberger, A. Guth, and D. Soper, Princeton University preprints.

69. A. M. Polyakov, Proceedings of the International Symposium on Lepton and Photon Interactions, Stanford (1975).